"From Monomeric to Dendrimeric MRI Contrast Agents"

Thesis by

Jakub Rudovský

For the Degree of

Doctor of Philosophy

Univerzita Karlova v Praze

Faculty of Science

Department of Inorganic Chemistry

Prague 2006

Table of Contents

Preface

$\mathfrak{A}$ desire to see insides of living objects non-invasively to observe how they are ordered and how they "work" could be tracked in the history of science and especially medicine since ancient times. At the end of nineteenth century, this desire seemed to be finally satisfied by the discovery of X-ray radiography. Quite soon it became clear that this tool despite its undoubted advantages was far from being harmless to living organisms due to accompanying ionizing radiation. In this context, the entrance of nuclear magnetic resonance (NMR) on the scene of physics and chemistry in mid-forties (of twentieth century) firstly did not attract too much attention. It had taken thirty years of a tremendous improvement in a knowledge, technology and informatics until scientists have realized an immense potential of the nuclear magnetism being a key to the completely new strategy of seeing beneath surfaces of biological objects nowadays known as <u>M</u>agnetic <u>R</u>esonance <u>I</u>maging (MRI). During that period of time, a progress in the NMR theory and application had been already awarded by three Nobel Prizes.[1] In order to foreshadow a history of MRI as it has been evolved on a background of NMR, it seems logical to start with the experiments of Dr. Raymond Damadian performed in the beginning of seventies on tissues dissected from rats.[2] Despite these observations were subject to significant instrumental imperfections, he concluded that a malignant and a healthy tissue differed significantly in magnetic relaxation times of water protons that could serve as an instrument for a visualizing of pathological changes in living subjects. The one of the founders of a modern MRI and later Nobel laureate Dr. Paul C. Lauterbur then remarked: "...*A phenomenon seemed to be at work there. But I couldn't imagine that it was very likely that it would be important to do such investigations of tissue. A method that required cutting out the samples didn't seem all that interesting...But it did seem useful if you could take measurements from the intact human body and create images...And I got to thinking that magnetic field gradients provide a general solution to this problem...*"[3] In fact, even before in 1972 Dr. Damadian filled the first MRI patent in history when he designed a 3D MRI apparatus for a scanning a whole human body for cancer (Figure 1).[4] The title of his patent read "Apparatus and Method for Detecting Cancer in Tissue".

The importance of Dr. Damadian's idea was quickly recognized and two independent groups of scientists led by the chemist Dr. Paul C. Lauterbur and the physicist Dr. Peter Mansfield published independently between 1973 and 1975 several experimental papers dealing with an application of NMR for a spatial imaging of objects (Figure 2).[5-8]

Both approaches have made use of a linear magnetic field gradient interacting with a sample placed in a static magnetic field. The new spectroscopic technique using a synergic effect of
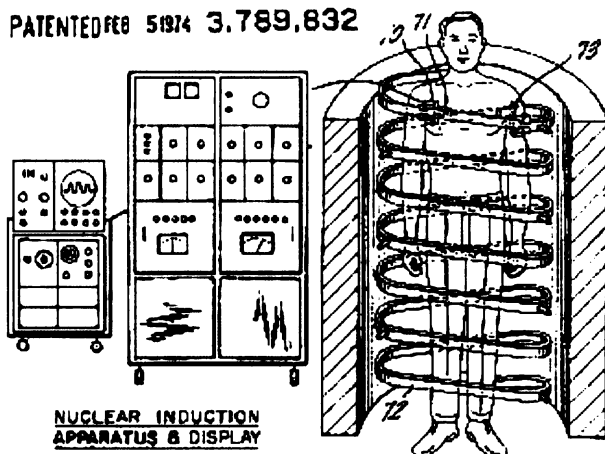
Figure 1. The figure was adopted from U. S. patent '832 of Dr. R. Damadian on 3D MRI scanner. The patent was filled on March 17, 1972.

both the static and the gradient field used for an encoding of spatial information was named "zeugmatography" (Greek word ζευγμα means "joining").[7] Both Dr. Lauterbur and Dr. Mansfield were awarded the Nobel Prize in Physiology or Medicine in 2003 for their fundamental discoveries concerning MRI.[1] The emerging method has been quickly improved thanks namely to a power of a computer driven Discrete Fourier Transformation (DFT) that was able to decode a 3D-phase encoded spatial information from a pulse-MRI experiment to generate a 3D image or a set of 2D slices.[9] The novelty and the profit from the applied DFT in NMR and MRI were later appreciated by another Nobel Prize award for Dr. Richard Ernst in 1991.[1] To demonstrate the huge exploitation of MRI since its beginning it may be noted that in 2003 there was ca. 22000 MRI scanners in use worldwide and more than 60 million MRI images were taken every year.

Logically, attempts to further enhance the quality of the images by an affecting the properties of a sample have paralleled the continual improvement of instrumental equipment since the beginning. A quality (i.e. a resolution and a contrast) of an MRI image originates not only from a hardware design but also from a spatial variation in physico-chemical properties of a studied tissue namely a local water concentration and proton magnetic relaxation times T_1 and T_2. In such a way, depending on an experimental set-up it is possible to get different types of images (Figure 3, ref [10]). As the concentration of

Figure 2. The first MRI image – famous Lauterbur zeugmatogram adopted from the Ref. 7. It depicts the 2D map of the proton concentration in a sample consisting of two water-containing capillaries placed in a standard 5 mm NMR tube.

water could be hardly influenced within tissues it was a subject of an intensive effort to influence the relaxation times of tissue protons by an administration of suitable contrast agents (CA).[11] The idea was not completely new as much earlier (in thirties) a Nobel Prize was awarded for the development of CA for X-Ray radiography.[1] It was discovered that, in principle, any paramagnetic substance like an organic radical or a suitable paramagnetic metal ion

5

might serve as a CA. Unfortunately, an injection of substances from both these classes as such would cause damage to living tissues due to their significant toxicity.

Orange tr=1s te=0.03s   Orange tr=7s te=0.5s
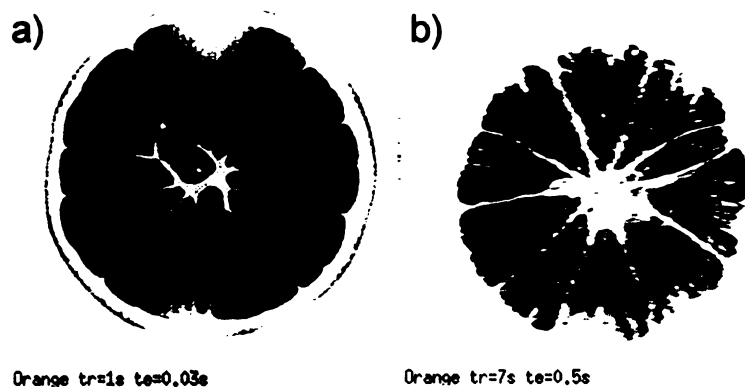
Figure 3. Examples of T_1-weighted (a) and T_2-weighted (b) MRI image. The sample here was an orange. The picture was adopted from Ref. 10. The colors of the images were digitally inverted.

Notwithstanding, the CAs based on compounds incorporating paramagnetic metal ions are nowadays administered in more than 30% of all MRI investigation and they have been proved to be not only extremely useful but also even essential in many types of MRI diagnosis. Moreover, it is really a hot field of current research to produce more efficient and more specific CAs for new emerging MRI applications as the molecular imaging. The present Thesis proposes to show a development I have made on several novel potential MRI T_1-contrast enhancing agents during my PhD period.

Abbreviations and Definitions

BSM	Bloembergen-Solomon-Morgan equations of paramagnetic relaxation
CA	contrast agent
Δ^2	trace of the zero-field splitting tensor
DIS	dysprosium induced NMR shift
DO3AP	1,4,7,10-tetraazacyclododecane-4,7,10-tris(carboxymethyl)-1-methylphosphonic acid
DO3A-P^{ABn}	1,4,7,10-tetraazacyclododecane-4,7,10-triacetic-1-{methyl[(4-aminophenyl)methyl]phosphinic acid})
DO3A-P^{NBn}	1,4,7,10-tetraazacyclododecane-4,7,10-triacetic-1-{methyl[(4-nitrophenyl)methyl]phosphinic acid})
DOTA	1,4,7,10-tetraazacyclododecane-1,4,7,10-tetraacetic acid
DTPA	diethylentriaminepentaacetic acid
LIS	lanthanide induced NMR shift
LS	Lipari-Szabo modification of Bloembegen-Solomon-Morgan equations
MION	microcrystalline iron oxides, synonymous to SPIO and USPIO
MRI	magnetic resonance imaging (tomography)
NMR	nuclear magnetic resonance
NMRD	nuclear magnetic relaxation dispersion
PAMAM	polyamidoamine dendrimers
q	number of water molecules bound in the first coordination sphere on Ln(III) ion
r_1	milimolar relaxivity, relaxation rate $1/T_1$ of 1 mM solution of contrast agent
R_1	longitudinal relaxation rate – $1/T_1$
R_2	transversal relaxation rate – $1/T_2$
SAP	square antiprismatic arrangement of coordination polyhedron
SPIO	small paramagnetic iron oxides
T_1	longitudinal relaxation time – $1/R_1$
T_2	transversal relaxation time – $1/R_2$
$^{(298)}\tau_M$	water residence lifetime (at 298 K) – reciprocal value to a water exchange rate k_{ex}
$^{(298)}\tau_R$	rotational or reorientation correlation time (at 298 K) also referred in the text as molecular tumbling time
TSAP	twisted square antiprismatic arrangement of coordination polyhedron
$^{(298)}\tau_v$	electronic correlation time (at 298 K)
USPIO	ultra small paramagnetic iron oxides
ZFS	zero-field splitting

1. Introduction

1.1 Overview of MRI Contrast Agents

Tomography of Magnetic Resonance (Magnetic Resonance Imaging - MRI) has gained a great importance in the last three decades in a medical diagnostics as an imaging technique with a superior spatial resolution and contrast.[11] The most important advantage of MRI over the competing radio-diagnostic methods like X-Ray Computer Tomography (CT) or Positron Emission Tomography (PET) is definitely its noninvasiveness as there is no convincing evidence of any long-term or irreversible subacute effects of MRI up to present time. Moreover, MRI often represents the only reliable diagnostic method for cranial abnormalities, multiple sclerosis and lesions detection. The resolution reached so far is close to 1 mm^3 with contemporary MRI clinical scanners, whereas the resolution of 1 μm^3 was demonstrated in a laboratory experimental setup. Consequently, the diagnostic potential of MRI seems to be still enormous. For instance, in a quite recent application, MRI has been used to follow functions of a human brain in a real time-scale by a method called functional-MRI or fMRI.[12]

Physical principles of MRI rely on a monitoring of a different distribution of water in an examined tissue and also on spatial variation of proton longitudinal, T_1, and transversal, T_2, magnetic relaxation times.[11] In respect to that, the MRI scanner is able to generate several types of images (Figure 1.1). An impact of MRI on medical diagnostics subsequently rises from a con-

Figure 1.1. The comparison of cerebral MRI images. From the left: proton-spin density, T_1 and T_2 weighted images. The picture on the right represents a T_1-weighted image where an extracellular T_1-CA was injected.

trast produced by local differences in water concentration and T_1 and T_2 relaxation times between healthy and pathologically changed parts of the same tissue. Especially T_1 and T_2 proved to be rather sensitive to a chemical condition (such as temperature, pH, salt or fat concentration) of the tissue under study.

During the time, it was found that in some examinations like in gastrointestinal tract (GIT) or cerebral scans, information obtained from an MRI image as such might not be sufficient. In

these cases, an administration of a suitable contrast-enhancing agent (CA) has proved to be extremely useful (Figure 1.1). Quite soon it was demonstrated, that the most promising class of CAs would be compounds comprising paramagnetic metal ions in some form and, in fact, the first CA ever tried *in vivo* was Cr(III) complex of EDTA (ethylenediaminetetraacetic acid).[13] Application of this highly paramagnetic substance (Cr(III) possesses 3 unpaired electron and magnetic moment 3.8 B.M.; B.M. = Bohr magneton = 9.274×10^{-24} JT^{-1}) induces much faster T_1 relaxation and surrounding tissue water appeared white in a T_1-weighted image. Unfortunately, this candidate suffered from a lack of a long-term stability and has never been used in clinics. As the first example of modern MRI contrast agent, the gadolinium complex of DTPA (diethylenetriaminepentaacetic acid) may be considered[14] approved for a clinical usage in 1988.

Nowadays, from physical point of view we distinguished two major families of CAs classified according to the relaxation process, which they predominantly accelerate, *i.e.* T_1-CAs (paramagnetic) and T_2-CAs (superparamagnetic).[11] Whereas T_1-CAs induce a positive contrast *i.e.* a ^1H NMR signal of an affected tissue increases, compounds affecting T_2 relaxation cause diminution of a local proton signal and, thus, they have a negative enhancement pattern.[15] Besides this classification, all CAs can be divided according to a site of action *e.g.* to extracellular, organ specific or blood pool (intravascular) agents. Historically, the chemistry of T_1-CAs has been explored more extensively as a T_1 relaxation time of diamagnetic water solutions is typically 5 times longer than T_2 and consequently easier to shorten.[11] From chemical point of view, T_1-CAs are complexes of paramagnetic metal ions like Fe(III), Mn(II) or Gd(III) with suitable organic ligands (Figure 1.2a). These agents can be administered as organ specific, blood-pool but mostly as extracellular CAs.

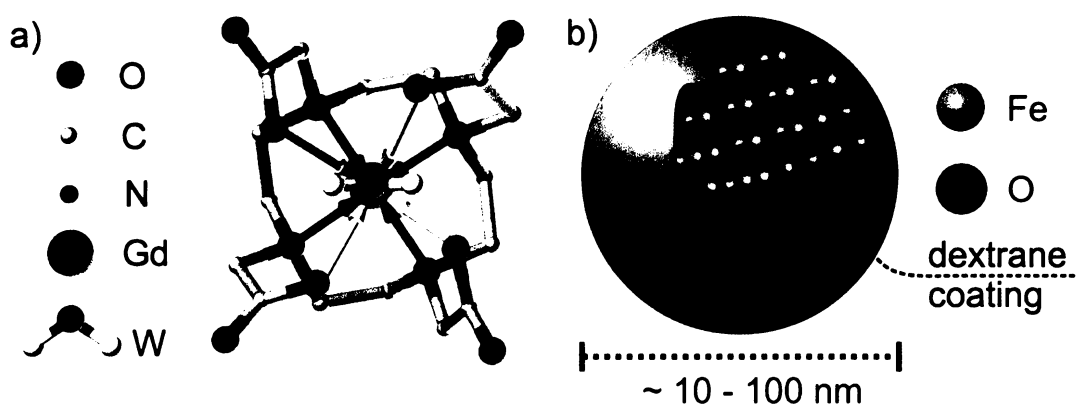**Figure 1.2.** The structural principles of (a) an extracellular Gd-based T_1-CA (Gd-DOTA complex) and (b) a generic MION-based T_2-CA structure.

On the other hand, the T_2-CAs, developed slightly later are conceptually microcrystalline iron oxides nanoparticles (MION) called also ultrasmall superparamagnetic iron oxides (US-PIO) or small superparamagnetic iron oxides (SPIO).[16] Additionally to their effect on T_2, these

compounds also induce faster T_1-relaxation and, in turn, they are often used both ways as negative and/or positive CAs. Basically, they are of various sizes covering a range from several nanometers to several hundred nanometers consisting of nonstoichiometric Fe_3O_4/Fe_2O_3 core coated with dextranes or siloxanes (Figure 1.2b). In practice, they are used as blood-pool and more recently as organ-specific CAs.

1.2 Gd - T_1 Contrast Agents

s was hinted above, T_1-CAs are mostly based on coordination compounds, where paramagnetic metal ion is wrapped around by a multidentate organic ligand. Nowadays, definitely the most exploited family of T_1-CAs is based on complexes of Gd^{3+} ion. Although, there are other candidates in the lanthanide series, the intrinsic relaxation time of electron-spin state has to match a Larmor frequency of protons at imaging field (20-60 MHz, *i.e.* 0.5–1.5 T) for the cation to be feasible for application in MRI. Thus, a prominent position of Gd^{3+} inheres not only in a high magnetic moment (7.9 B.M.) given by seven unpaired f-electrons but also in a totally symmetric electronic state (ground state - $^8S_{7/2}$) that makes an electronic relaxation time in just optimal range, $10^{-8}–10^{-9}$ s.[17] However, the main problem with heavy metal ions like Gd^{3+}, is their significant toxicity if applied in a "free" (aqua ion) form. Particularly, the toxicity of lanthanide(III) ions is caused either by a precipitation its hydroxides or formation of salts with biogenic anions like carbonate, phosphate or citrate in plasma. Thus, to use gadolinium(III) clinically, it needs to be bound in form of complex endowed with a high thermodynamic stability and, even more importantly, it must show a long-term resistance toward a transmetallation loss of Gd(III). In this respect it was proved that from the endogenous metal ions, Zn(II) and Ca(II) were the main competitors and thus the candidate ligand has to show a high selectivity for Gd(III) over these two cations.[18] In this light, the most important toxicological feature of the complex is the rate of transmetallation in comparison with a rate of excretion. From the structural point of view, two types of organic ligands have been developed, namely 12-membered tetraazamacrocyclic and acyclic polyamines with several chelating pendant arms.[11] Selected clinically used CAs based on Gd(III) complexes are shown in Chart 1.1 and their relevant pharmacological characteristics (stability constant, typical application dose, indication and pharmacokinetic data) are comprised in Table 1.1.

10
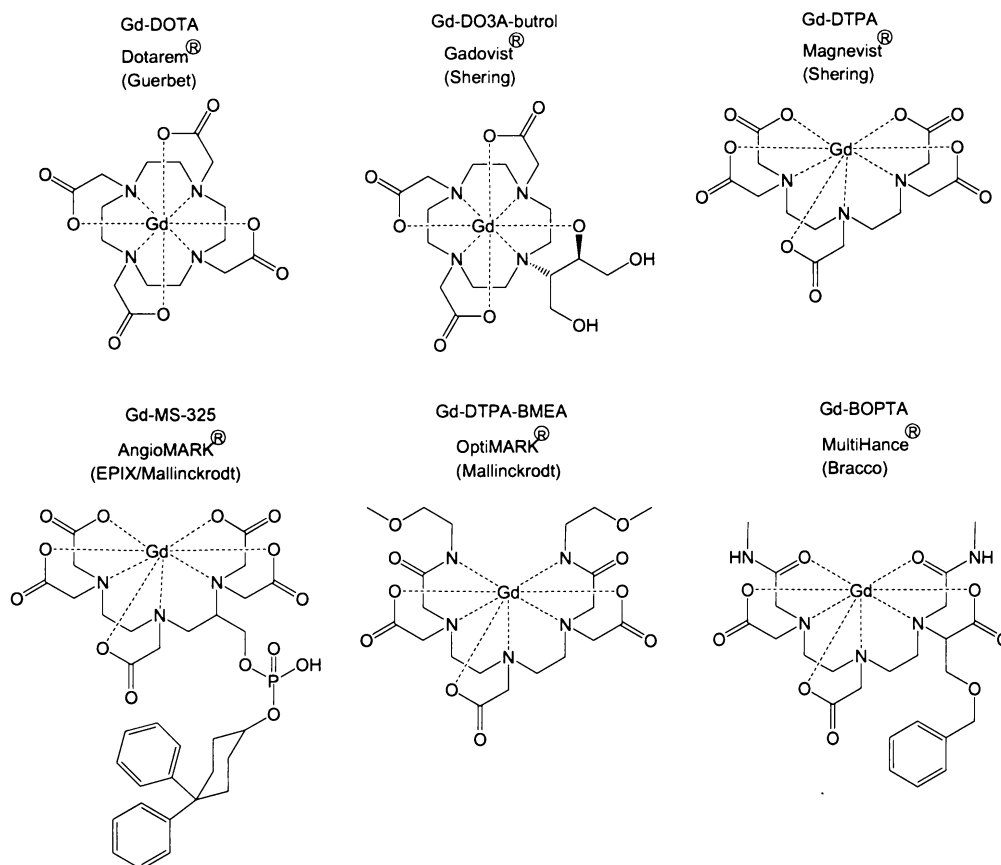
Chart 1.1. Selected clinically used contrast agents. In the chart, there are shown only Gd-containing parts instead of full chemical formula. Coordination water molecules were also omitted for clarity.

Table 1.1. Relevant characteristics of selected clinically used Gd(III)-based contrast agents.

Gd(III) complex of	$\log K_{GdL}$	application dose [g/for 80 kg][a]	distribution time / elimination halflife [min]	excretion rate	indication	ref.
DOTA	25.3	4.6	NF	NF	CNS/body	19,20
DTPA	22.46	7.5-22.4	12/100	86% / 6 h	CNS/body	21,20
DO3A-butrol	21.8	5.0	15/45	94% / 24 h	CNS/body	20,22
MS-325[b]	22.06	2.1	NF/120-180	NF	blood pool	23,20,24
DTPA-BMEA	16.84	5.3	13/104	96% / 24 h	liver/CNS	25,20
BOPTA	22.59	4.2–8.5	NF	NF	liver/CNS	26,20

[a] typical doses are 0.03 mmol/kg for MS-325 and about 0.1 mmol/kg for the other mentioned CAs; [b] the commercial name MS-325 represent Gd(III) complex but could be used for pure ligand as well; NF = not found

An overall coordination number of Gd^{3+} ion in all these complexes is 9 leaving one coordination site for water molecule that is crucial for contrast enhancement mechanism (see below). Additionally, the structure of the ligand could be further modified to tune organ selectivity or an excretion pathway. For example, low molecular negatively charged complexes diffuse within few minutes after injection into intravascular and extracellular compartments over a whole body. Importantly, they diffuse to cerebral tumors and also are allowed to penetrate a broken

brain-blood-barrier (BBB) *e.g.* in certain stages of multiple sclerosis. Finally, these agents undergo a glomerular filtration in kidneys and they are renally excreted in a few hours. Thanks to the relatively broad distribution of these agents, it is necessary to administer rather high doses: typically about 5 g of CA in 15 ml for 80 kg of the weight. This might be a drawback because multiple-charged complexes with a high osmolalities cause painful osmotic shock in vicinity of the intravenous application site. Noteworthy, X-ray contrast agent for angiography are injected even at higher doses and the administration is mostly much more painful. To the contrary, complexes bearing non-polar groups remain in blood for a longer time and they are caught off by livers and excreted much slowly by a hepatobiliary excretion. Hence, these agents are suitable for a mapping of the vascular system and liver lesions.[27]

1.3 Efficacy of Contrast Agents

The efficacy of CA measured as an ability of its 1 mM solution to increase longitudinal relaxation rate R_1 (= $1/T_1$) of water protons is called relaxivity labeled r_1.[11] Unfortunately, all commercially used T_1-CAs show a quite low relaxivity, about 5 $s^{-1}mM^{-1}$, whereas according to the established theory (Bloembergen-Solomon-Morgan or BSM model) more than 20 times higher value can be attained by an optimization of parameters governing the relaxivity though a structure of complex. Logically, a tuning of a ligand structure is the field of an intensive research for last 20 years because an increase of the efficacy will allow a dramatic decrease of an application dose. Additionally, only highly efficient CAs are feasible for applications such as targeted MRI probes for the molecular imaging. The overall relaxivity can be correlated with a set of several physico-chemical parameters, which describe a complex structure and dynamics. Those, which could be chemically tuned, are of primary importance in the ligand design(Figure 1.3).[28]:

(i)   number of inner-sphere water molecules directly coordinated to Gd(III) center – q

(ii)   water residence lifetime of the coordinated water molecule – τ_M

(iii)   rotational correlation time representing a molecular tumbling time of a complex – τ_R

(Full BSM equations including their description are presented in Appendix 1.)

The relaxivity of CA is linearly dependent on q but, in principle, its value cannot be raised above 2 without a considerable loss of *in vivo* stability. Another option is to modify a ligand to benefit from contributions given by so-called second- and outer-sphere hydration shell. A complex may tend to align surrounding water molecules either by a hydrogen-bond network[29–32] or they just get to a close vicinity of a paramagnetic ion by mere diffusion motion creating the
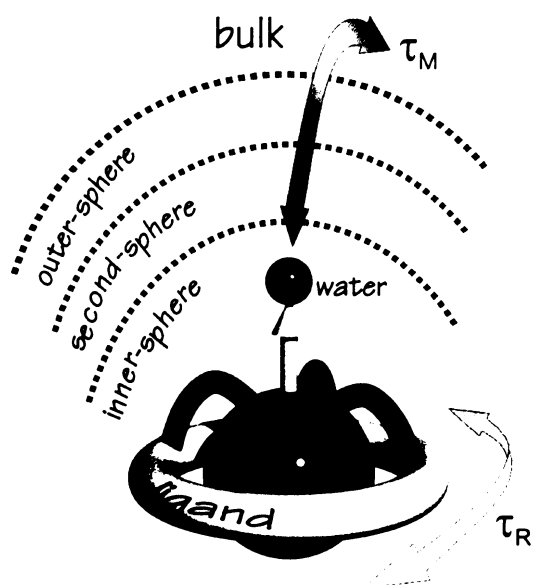
Figure 1.3. Model of Gd-based CA in solution.

second-sphere or the outer-sphere hydration shell, respectively. Both these kinds of water molecules may contribute to the overall relaxivity quite significantly. However, manipulation with an inner-sphere contribution representing typically about 60% of the relaxivity is much more straightforward.

The simulations at Figure 1.4 demonstrate the dependence of relaxivity on τ_M and τ_R at given imaging fields and values of electronic relaxation parameters.

A typical values of parameters for contemporary T_1-CAs used in clinics are about 1×10^{-7} s for τ_M and 1×10^{-10} s for τ_R whereas an optimal values should be about 1×10^{-8} s for τ_M and minimally 1×10^{-8} s for τ_R.[11] In other words, a structure of a complex needs to be tuned to allow one order of magnitude faster water exchange and by two orders of magnitude slower molecular tumbling. Moreover, by inspecting the Figure 1.4, it can be moreover noticed that the optimal water residence lifetime as well as maximally attainable relaxivity decreases with an increasing intensity of the imaging field. Whereas, the former issue can be addressed by a ligand design, the later one, unfortunately, lies "deep" in physical principles of the magnetic relaxation and as such cannot be influenced chemically. This point is of a special importance as current imaging field intensities range from 0.3 T to 3 T and commercial suppliers of MRI instrumentation already invest in 4.7 T, 7 T and even 11.7 T systems.[33] Another aspect that is out of chemical reach is an electronic relaxation of a Gd^{3+} ion. As was mentioned above, its rate is crucial for the efficacy of the magnetic information transfer from a paramagnetic metal center to water protons: if the electronic spin-state changes too fast, protons are virtually decoupled and the overall relaxivity is low. Within generalized BSM (GBSM) theory (see Appendix 1), the electronic relaxation rates, $T_{1e,2e}$, are mainly determined by a magnitude of zero-field splitting (ZFS) of symmetrical $^8S_{7/2}$ ground state of the Gd^{3+} ion. In BSM model, the ZFS is given firstly by a deviation of a coordination polyhedron from a regular octahedral shape (giving rise to static ZFS contribution) and then, by random collisions of a complex with molecules of solvent water producing transient disturbations (transient ZFS).[34] The static contribution is dependent on τ_R and thus highly relevant for slowly tumbling molecules. The transient term is described by its "amplitude", $\Delta^2 = $ the trace of ZFS tensor, and by a corresponding electronic modulation time, τ_v.[28] Unfortunately, despite the values of these parameters depend intrinsically on a ligand structure, they can be hardly predicted on rational basis until now. Moreover, the theory describing

Figure 1.4. The simulations of relaxivity as a function of a water residence lifetime, τ_M, and a rotational correlation time τ_R at an imaging field 20 MHz of a proton Larmor frequency *i.e.* 0.5 T (a,b) and 60 MHz *i.e.* 1.5 T (c,d). The amplitude of ZFS, Δ^2, was fixed to 0.05 × $10^{20}s^{-2}$ customary for macromolecular systems (a,c) and 0.5 × 10^{20} s^{-2} customary for low-molecular systems (b,d). The correlation time for a modulation of ZFS was fixed to 10 ps in all cases.

the electronic relaxation of macromolecular systems (long τ_R) is still not fully adequate that complicates an evaluation of relaxometric data.[35]

1.4 Rational Design

As it was already mentioned, except a hydration number q, a water residence lifetime, τ_M, and rotational correlation time, τ_R, are the only parameters having a high impact on r_1 that could be effectively addressed by a ligand design. Table 1.2 summarizes the values of τ_M and τ_R for selected CAs.

Table 1.2. The relevant relaxometric characteristics of the selected gadolinium(III) complexes shown in the Chart 1.1 and 1.2.

Gd(III) complex of	q	r_1 [s^{-1} mM^{-1}]	$^{298}\tau_M$ [ns]	$^{298}\tau_R$ [ps]	ref.
DTPA	1	3.7^a	303	80	36
DOTA	1	3.4^a	243	72	36
MS-325	1	6.6^a	72	100	35
BOPTA	1	4.4^a	290	88	26
S-SSS-NO$_2$BnDO3MA-1A	1	5.7^a	6	113	37
PCTA	2	6.9^b	70	70	38
2HM-TREN-Me-3,2-HOPO	2	10.5^b	16	129	39
TRITA	1	NF	4	82	40
DO3A-pyNox	1	4.0^a	39	74	41
aqua ion	8	11^a	1.2	41	36

^{a} 20 MHz, 37 °C; ^{b} 20 MHz, 25 °C; NF – not found

As it was also mentioned above, most of the currently used CAs suffer from a non-optimally long water residence lifetime. Not surprisingly, a tuning up of τ_M was an issue chemists have been focused on since the beginning of the rational CA design. On the basis of a huge collection of data, several principles connecting structural properties of the ligand with water exchange rate ($k_{ex} = 1/\tau_M$) have been discovered. Interestingly, in spite of original beliefs that the water exchange rate will be approximately the same or even faster for the gadolinium(III) complexes than that for [Gd(H$_2$O)$_9$]$^{3+}$ aqua ion, water exchange rates of known Gd(III) systems are generally lower and cover a range of 4 orders of magnitude.[27] It was proved that at given coordination number (CN), the exchange rate depends on lanthanide(III) ion radius: passing from Gd(III) to Yb(III) in octacoordinated aqua ions, the exchange rate decreases by more than one order of magnitude. This trend is followed by a change of activation volumes $V^{\#}$ from strongly negative toward zero indicating a shift from pure associative mechanism (A) to slower associative interchange pathway (I$_A$); a decreasing the ion radius levels up the energy of an activated nine-coordinate state that, in turn, increases an overall free energy of the water exchange. Similarly, for lanthanide(III) complexes of simple ligands like PDTA (propylenediamine-tetraacetate), the water exchange rate varies with Ln(III) ionic radius: the light lanthanides prefer generally fast associative mechanism whereas the heavy ions adopt much slower dissociative pathway.[42] Unfortunately, Gd(III) complexes with octadentate DOTA-like ligands and one capping water molecule generally follows slower dissociatively activated interchange (I$_d$) pathway. The difference between associative and dissociative exchange mechanism could be witnessed by the comparison of $^{298}\tau_M$ for the Gd(III) complexes of DOTA (dissociative - 234 ns)[36] and hexadentate HOPO-type (hydroxypyridonate, $^{298}\tau_M$ typically 8-20 ns, associative mechanism)[39]

Gd-S-SSS-NO₂BnDO3MA-1A

Gd-PCTA

2HM-TREN-Me-2,3-HOPO
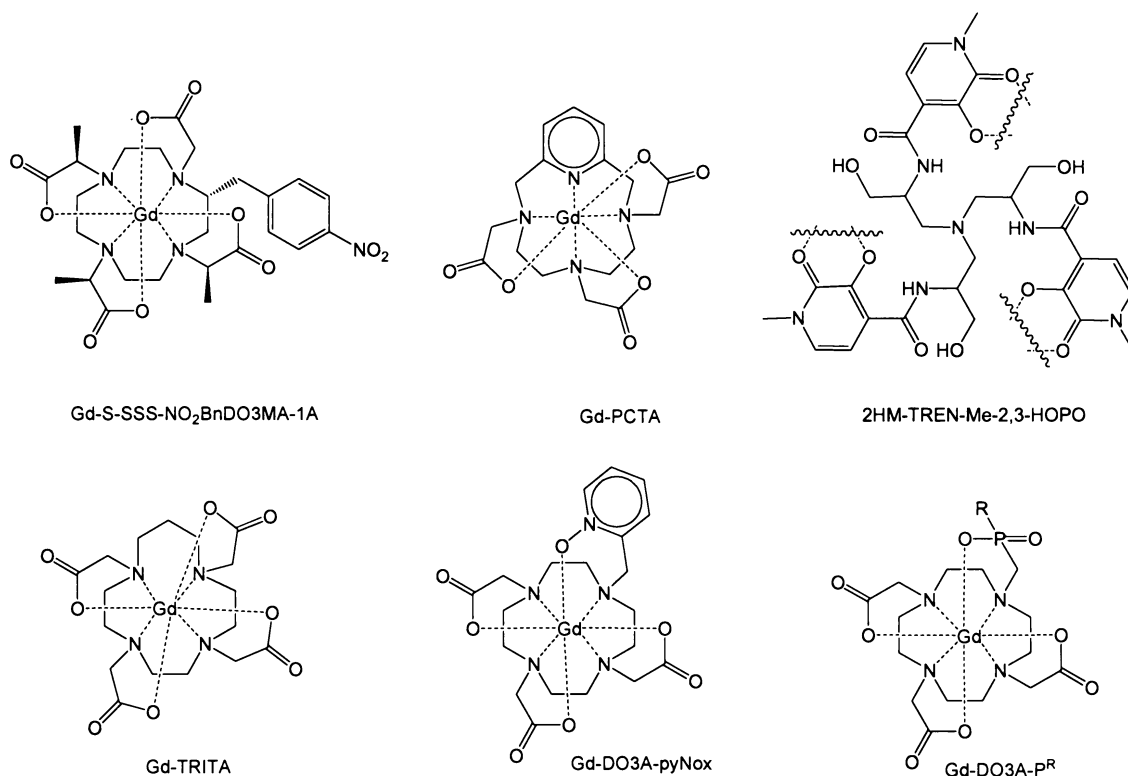
Gd-TRITA

Gd-DO3A-pyNox

Gd-DO3A-P^R

Chart 1.2. The ligands discussed in the text and comprised in the Table 1.2.

or heptadentate PCTA ligands (pyridine-containing triacetate, $^{298}\tau_M$ 70 ns) (Chart 1.2).[38] In order to accelerate a water exchange in the systems adopting the dissociative mechanism, several strategies have been developed. General approach relies on an introduction of a steric compression around the water-binding site. For example, by an enlargement of cyclen backbone to a 13-membered macrocyclic ring in TRITA (Chart 1.2),[40] it was achieved 60-fold reduction of water residence lifetime, τ_M, over that reported for Gd-DOTA ($^{298}\tau_M = 243$ ns). Another option stems from a knowledge that Ln-complexes of DOTA-like ligands occur in solution as a mixture of two diastereomeric forms differing by orders of magnitude in water exchange rate (see below). For instance, it was demonstrated on Gd-complex of α-alkylated bifunctional derivatives of DOTA, NO₂BnDOTMA (NO₂BnDOTMA = 1,4,7,10-tetraazacyclododecane-2-*p*-nitrobezyl-1,4,7,10-tetra-2-propionic acid)[43] and more recently on its NO₂BnDO3MA-1A analogue[37] (Chart 1.2)), the pure isolated *S-SSSS* forms exhibited rather fast water exchange as $^{298}\tau_M$ was found to be 15 ns[43] and 6 ns[37], respectively where their corresponding diastereomers showed values of 120 and 70 ns, respectively. In our group, we have shown that introducing a six-membered chelate ring into the complex structure could also increase a steric crowding on the apical water-binding site and, in turn, have a positive effect on the water residence lifetime. We have proved this principle in the case of pyridine-*N*-oxide derivative of DO3A, DO3A-py*N*ox (Chart 1.2) showing $^{298}\tau_M$ of 39 ns.[41] In this Thesis, it will be presented also another approach how to manipulate with a water exchange: we observed that properties of a chelate might be

16

remarkably improved by substituting one carboxylate group by a more sterically demanding phosphonic or phosphinic acid.

In systems with optimized τ_M, the overall relaxivity is controlled by the rotational correlation time. Figure 1.5 depicts the simulations of relaxivity profiles as a function of τ_R at fixed values of the electronic parameters and a water residence lifetime. In order to slow down the reorientational motion of gadolinium (III) complexes, several
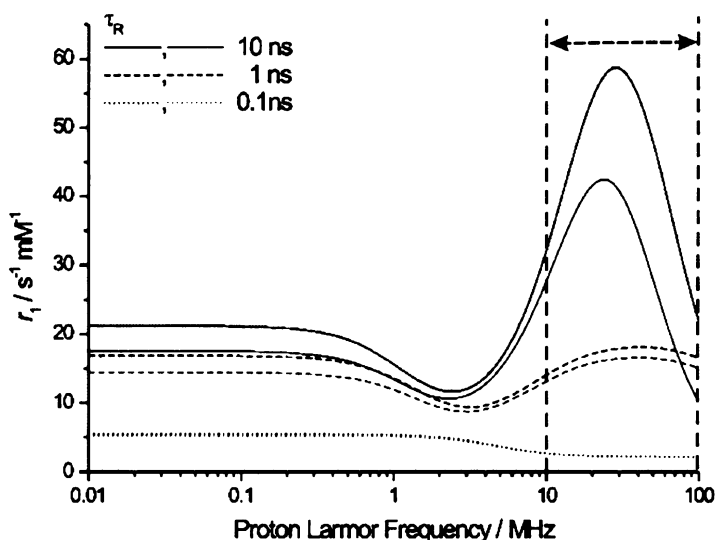
Figure 1.5. The simulations of relaxivity as a function of proton Larmor frequency (NMRD profile) at $^{298}\tau_M$ set to 10 ns (black lines) and 500 ns (red lines) and $^{298}\tau_R$ set to 100 ps, 1 ns and 10 ns. The values of the other relaxometric parameters were set to common values: $T = 37\ °C$, $^{298}\tau_v = 40$ ps, $\Delta^2 = 0.1 \times 10^{20}$ s^{-2}, $R_{GdH} = 3.1$ Å. The blue area shows the range of imaging fields currently used in clinics.

techniques have been used. Conceptually, they represent different strategies how to increase an effective molecular weight of such systems. For instance very recently, it was demonstrated that bulky substituents like polyethyleneglycol-based (PEG) dendrons attached to macrocyclic pendant arms can effectively act like "molecular brakes" slowing down the motion of the system from typical 100 ps up almost 400 ps.[44,45] A different way uses a combined-micelle formation of complexes conjugated to hydrophobic aliphatic or terpenoid moieties, phospholipides and suitable surfactant (see Figure 1.6).[46-49] This approach may lead to increase of τ_R up to 3 ns. However, the most general strategy relies on covalent or non-covalent conjugation of low-molecular

non-covalent protein
adduct

combined micelle

covalent dendrimeric
conjugate

Figure 1.6. The sketch of selected types of "immobilization" of low-molecular Gd(III) complexes. The generic Gd(III) complexes are represented by the green spheres.

species to a suitable macromolecular carrier (Figure 1.6). The main advantage of the conjugation, except its versatility, lies in the possibility to improve not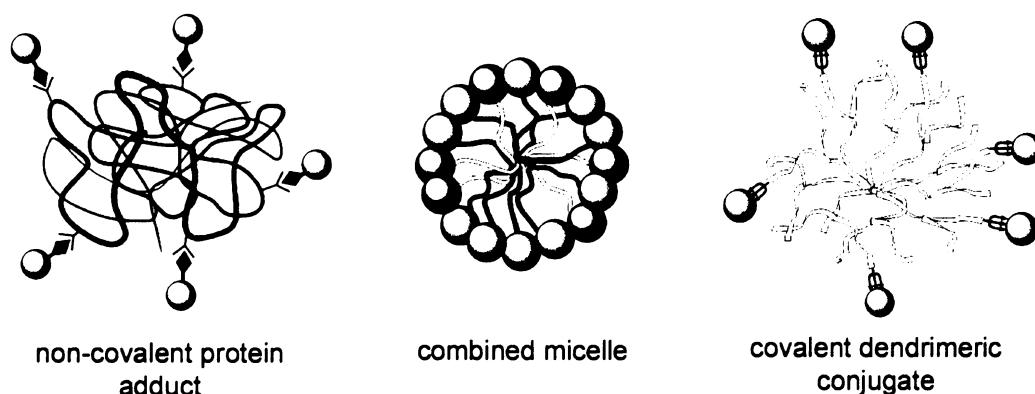 only the relaxometric properties of Gd(III) complex but also pharmacological aspects like a biodistribution.[27] As a nice example of application of the non-covalent approach could be mentioned the Gd(III) complex MS-325 (Chart 1.1) designed for angiography. The principle of action lies in a strong non-covalent interaction of the bis(phenyl) group of the ligand with blood human serum albumin (HSA).[50] As a macromolecular carrier able to transport CA to targeted tissue may also act a artificial polymers, dendrimers or, eventually, an antibodies (see Figure 1.6 and Chapter 1.7).

Relaxivity of macromolecular or supramolecular CA adepts may be hampered basically for two reasons. Firstly, due to the complexity of the system, the water exchange process is decelerated even though the free Gd(III) complex itself exhibits a fast water exchange[51]; unfortunately, as the molecular weight of such system grows up, a negative impact of slow water exchange levels up (Figure 1.5). The second limiting factor is an internal flexibility of the system. This is crucial especially for polymeric and dendrimeric covalent conjugates, where the global motion of the molecule is not fully coupled with the relaxivity; in result, the overall r_1 is more influenced by the superimposing internal motion. DTPA and DOTA conjugates with polyamines or polyamidoamine dendrimers (PAMAM) may be considered as an example; a "saturation" of the relaxivity with an increasing size of the system was reported[52,53] (this subject will be discussed in more details in Chapter 3.4).

1.5 Structure of Lanthanide(III) Complexes with DOTA-like Ligands

It was already hinted, that the lanthanide(III) complexes of DOTA-like ligands occur in solution in mixture of isomers.[54,55] That is caused by two degrees of freedom in a ligand geometry after the complex formation: (i) the ethylene bridges may concertedly interconvert, likewise in simple EDTA complexes, giving rise either to $\lambda\lambda\lambda\lambda/\delta\delta\delta\delta$ isomers and (ii) the pendant arms may rotate clockwise or counterclockwise in respect to the "nitrogen plane" creating Δ/Λ isomers. In combination, the ring inversion and the arm rotation produce four arrangements $\Lambda(\lambda\lambda\lambda\lambda)$, $\Delta(\delta\delta\delta\delta)$, $\Lambda(\delta\delta\delta\delta)$ and $\Delta(\lambda\lambda\lambda\lambda)$: two enantiomeric pairs of diastereoisomers (Figure 1.7). From the structural point of view, the $\Delta(\delta\delta\delta\delta)$ and $\Lambda(\lambda\lambda\lambda\lambda)$ isomers adopt the twisted-square antiprismatic conformation (TSAP) where the "oxygen" and the "nitrogen" planes are mutually rotated ideally by 22.5°. Then the $\Delta(\lambda\lambda\lambda\lambda)$ and $\Lambda(\delta\delta\delta\delta)$ isomers adopt the square-antiprismatic conformation (SAP) with the oxygen (O4) plane rotated ideally by 45° in respect to the nitrogen plane (N4)(Figure 1.8). All these isomeric forms may exist in a dynamic equilibrium in solution that allows identifying two sets of NMR signals: each set for one enantiomeric

Twisted square antiprism
Δ(δδδδ)

Square antiprism
Λ(δδδδ)

Arm
Rotation

Ring Inversion

Ring Inversion

Arm
Rotation

Square antiprism
Δ(λλλλ)

Twisted square antiprism
Λ(λλλλ)
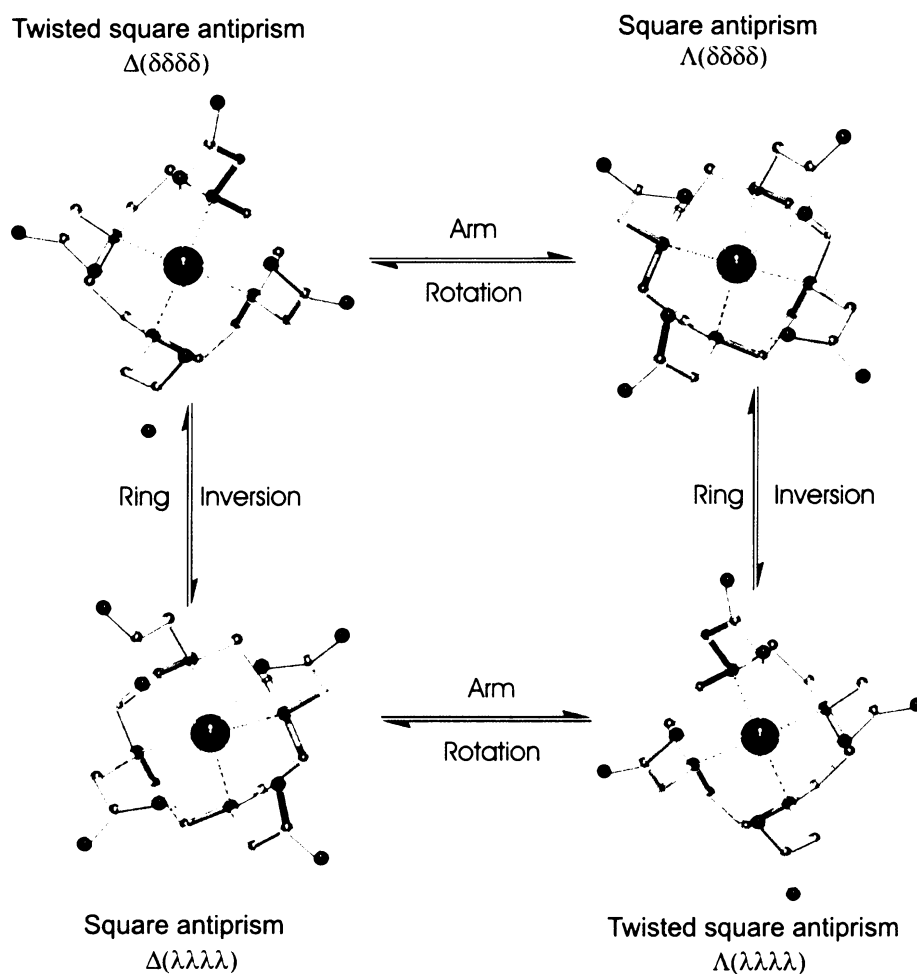
Figure 1.7. The summary of the interconversion pathways for Ln-DOTA complexes.

pair. Both arrangements significantly differ not only in the rotation angle but also in the distance between O4 and N4 planes: for SAP, it is typically in quite a narrow range around 2.35 Å whereas in more variable TSAP it can lie anywhere between 2.5 and 2.8 Å.[56] In consequence, the TSAP-structure is preferred by the lighter lanthanides with the larger ionic radii and, conversely, complexes with the heavier lanthanides occurs predominantly in SAP-structures. In the solution, a TSAP/SAP ratio typically shifts along the lanthanide series from exclusivity for the TSAP-form in the beginning of the Ln-series to a dominance of the SAP-form at its end. This may be nicely witnessed in the DOTA complexes where 100% abundance of the TSAP isomer was found for the La(III) and Ce(III) complexes, whereas for Gd(III) it was only about 20%.[54,55] Likewise, in the solid state for Ln-DOTA complexes, the TSAP structures were found for La and Ce complexes, whereas for Eu(III), Gd(III), Dy(III), Ho(III) and Lu(III) only SAP structures are known.[57-61]

Importantly, it was found that as TSAP form is more compressed it expunge a coordinated water molecule more efficiently and thus, the TSAP isomers exhibit 10-1000 times faster water exchange.[62] The comparison of $^{298}\tau_M$ for the S-SSSS (TSAP) and S-RRRR (SAP) isomers of

19

Twisted square antiprism   Square antiprism

$\phi = 144°$ $\phi = 148°$

d = 2.52 Å   d = 2.36 Å

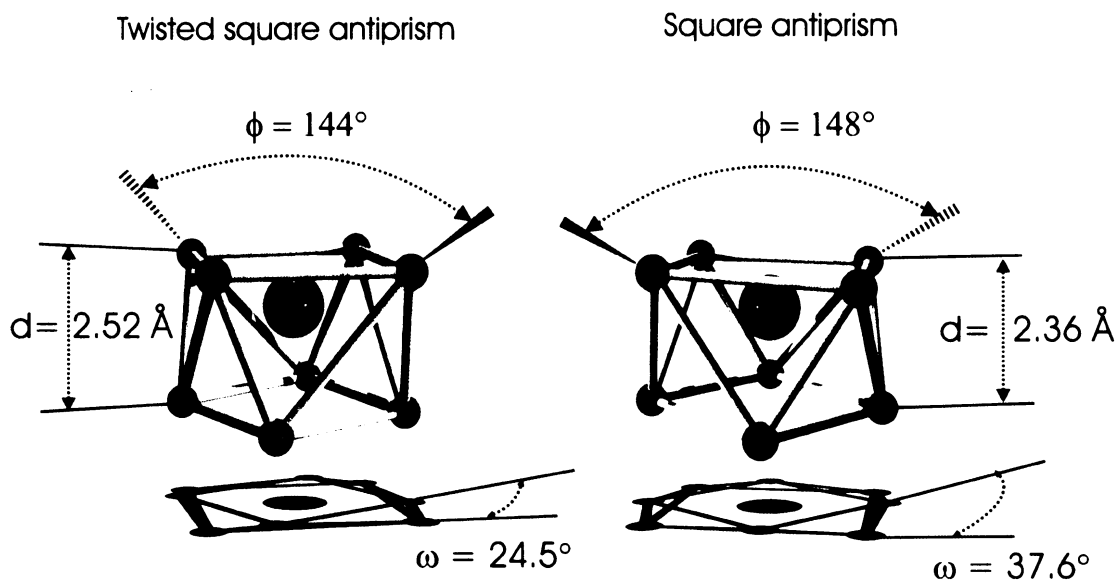$\omega = 24.5°$ $\omega = 37.6°$

Figure 1.8. The coordination polyhedrons of the TSAP and SAP isomers based on the X-ray structures of the Ce(III) and Pr(III) DOTA complexes. The coordinated water molecules are omitted for the clarity. Oxygen atoms are depicted in red, nitrogen atoms are in blue and lanthanides in green. The ω represents the average mutual rotation angle between O4 and N4 planes, d is the distance between O4 and N4 plane centroids and ϕ is the average value of the O-Ln-O opening angle.

NO$_2$BnDO3MA-1A where the values 6 ns and 70 ns[37] were reported may serve as the recent example

Such a significant difference in τ_M have fostered a ligand design to achieve as high TSAP abundance for a Gd(III) complex as possible. In this regard it was observed, that a presence of a bulky phosphorus-containing moiety shifts the isomeric equilibrium in favor to the TSAP-form even for the heavier lanthanides. This is usually ascribed to higher steric demands of a phosphorus-containing group over carboxylate. For instance, it was demonstrated that in tetraphoshorus ligands like DOTP (Chart 1.3) where all four carboxylate groups of DOTA were replaced by phosphonates, the Ln(III) complexes occur exclusively in the TSAP-form along the whole Ln-series, both the solution and the solid-state; but unfortunately, the complexes lack the coordinated water molecule.[63,64] An introduction of pro-chiral phosphorus groups (a phosphinate or a phosphonate half-ester) gives rise to a new chiral centre at the phosphorus atom upon coordination and the number of possible isomers is increased (see Chapters 3.2 and 3.3). Particularly, substitution of one phosphinate and/or phosphonate monoester for carboxylate splits each original isomer to R and S epimers with a new chiral centre at the phosphorus atom. This gives rise to four pairs of enantiomers in total. The situation is even more complicated by replacing all carboxylates like in DOTPPh DOTPME or DOTBzP (Chart 1.3). Lanthanide(III) complexes of these ligands prefer TSAP coordination manner, however, six different configurations at the phosphorus atoms could be distinguished, namely *RRRR*, *RRRS*, *RSRS*, *RRSS*, *SSSR* and *SSSS*. Additionally, the phosphorus arms may still wrap (in concerted manner with a ring-inversion in

20
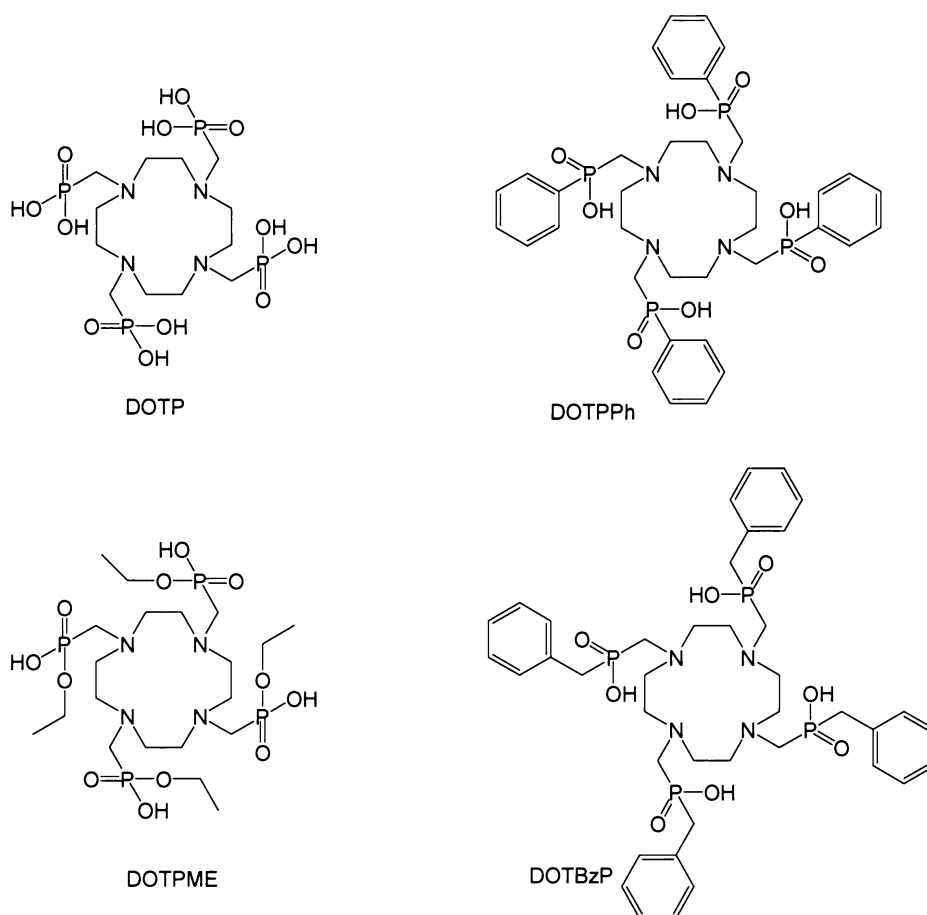
Chart 1.3. The structures of the discussed tetraphosphorus ligands

this case to preserve TSAP-form) clockwise or counterclockwise (Δ or Λ). Combining both isomerisms, six pairs of enantiomers (*e.g.* Δ-*RRRR* and Λ-*SSSS* are enantiomers) may exist in solution.[65] This was proved by solution NMR study for DOTPMeP[66] or DOTPP[67], whereas in some cases (*e.g.* DOTBzP) a specific arrangement (*RRRR* or *SSSS*) is preferred.[63]

1.6 Covalent Conjugates as Contrast Agents

Covalent conjugation represents one way how to improve the biophysical (relaxivity, rotational correlation time) and pharmacological properties (organ specifity, elimination time and elimination pathway) of MRI contrast agents.[68] Conjugation procedure is usually based on the reaction of an activated chelate with a primary amine or thiol group of a macromolecular reactant. The most common chemistry involves acylation, alkylation, urea and thiourea formation (Chart 1.4).[69-72] In majority, the commercially available ligands like DTPA and DOTA are modified to active esters and than conjugated to a polymer *via* amide bond. The octadentate coordination fashion is preserved in this way however, the change of carboxylate to amide have

very often a negative impact on relaxometric properties; amid exhibited significantly decelerated water exchange rate[11] and, moreover, the affinity of the modified ligand toward Gd(III) may be substantially decreased.[73] More promising way seems to be a design of bifunctional ligands where the linking group is attached directly to the ligand backbone. The most common reaction scheme includes a preparation of a ligand derivatized by a nitrobenzyl group followed by a subsequent modification to a highly reactive isothiocyanate (Chart 1.4).

For the artificial macromolecular carriers, linear polylysines (PL)[71,74] or dendrimers based on polylysine or polyamidoamine (PAMAM)[53,75] structures of a different size have been used. The main advantage of the dendrimeric conjugates over the linear polymeric ones stems from their more branched and, thus, rigid structures; as the segmental motion is limited, the global motion contributes more to the overall relaxivity. This could be nicely demonstrated by the comparison of their relaxivities: the relaxivity for PL-based agents vary in range
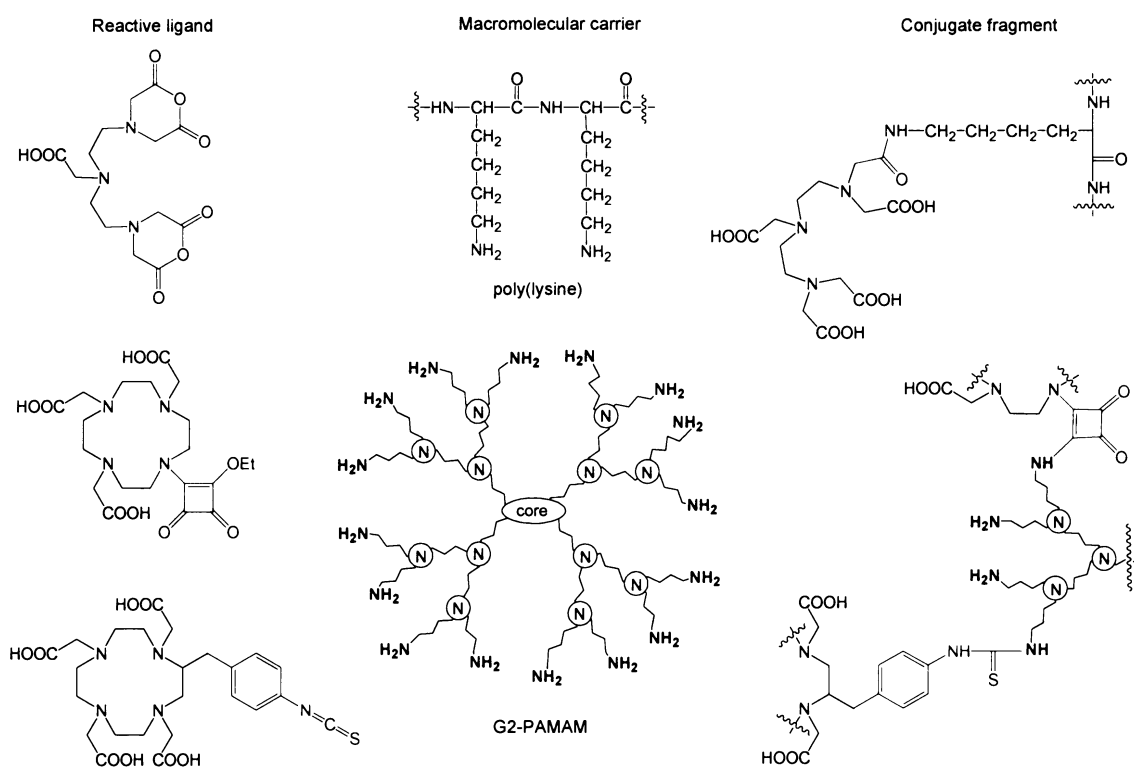
Chart 1.4. Selected examples of the conjugation strategies and corresponding synthons.

15–20 s^{-1} mM^{-1} whereas for PAMAM-based agents, the values of r_1 up 34 s^{-1} mM^{-1} were achieved. In addition, potential dendrimeric-based MRI CAs would benefit from their narrow distribution of molecular sizes (*i.e.* low polydispersity).[76]

The other class of macromolecules consists of those occurring naturally like peptides (albumines)[77] or polysaccharides (dextranes).[78] The special class of compounds is targeted agents conceptually based on Gd(III) complexes attached to monoclonal antibodies or other receptor-

specific moieties.[79] However, the covalent conjugation chemistry is, in principle, the same and these compounds, yet in development, are not used clinically, so far; it is mostly due to a complexity of preparation, high cost and only a moderate distribution enhancement in comparison with simple CAs so far.

2. Scope of the thesis

Various features of the agent running for the "holy grail" among the contrast agents were introduced in the first chapter. From a biophysical point of view, the candidate should be endowed with an optimal rate of water exchange and with the longest possible rotational correlation time. The usual course of research aims to design a low-molecular precursor with an optimized water exchange dynamics and appropriate thermodynamic stability and kinetic inertness. Having that managed, it is common to slow down the molecular tumbling by a suitable conjugation strategy in the next step. In the same time, the pharmacologic properties like a tissue distribution and/or retention of the agent could be adjusted.

In the present work, I explored what advantage in the CA development could be reached by a replacement of one carboxylic group in the DOTA structure with a phosphorus acid moiety. The study was carried out in a stepwise fashion: the first structure I studied was the simple monophosphonate analogue of DOTA and its lanthanide(III) complexes. Then, the phosphonate was changed for benzylphoshinates DO3A-P^{NBn} and DO3A-P^{ABn} that is and able to be covalently bound to a macromolecule via the benzyl side-chain attached to the phosphorus atom. In the next step, the model conjugate was prepared by joining two DO3A-P^{ABn} units; the effect of the conjugation on relaxometric properties was then studied on this ditopic structure. Finally, the DO3A-P^{NCS} unit was conjugated to several starburst dendrimers of the PAMAM family.

The results obtained within my Thesis are discussed in the following "Results and Discussion" part divided in to four chapters. The first part (Chapter 3.1) deals with the 12-membered macrocyclic ligand DO3AP (Chart 2.1, monophosphonate analogue of DOTA) and it is covered by the paper reprinted in the Appendix 2. In this chapter, the solution structure of the lanthanide(III) complexes with DO3AP is discussed and, in particular, the TSAP/SAP isomerism analyzed extensively in the paper is revisited. The second part of this chapter is focused on pH-variable relaxometric characterization of the Gd-DO3AP complex.

Chapter 3.2 concerns the solution study on the bifunctional ligand DO3A-P^{ABn} (and its synthetic precursor DO3A-P^{NBn}) (Chart 2.1, monophosphinate analogue of DOTA). Since this ligand was primordially designed for a preparation of high-molecular Gd(III) complexes as a candidates for MRI contrast agents, the relevant relaxometric solution-structure characteristics of its Gd(III) complex were studied. The investigation on DO3A-P^{ABn} has been published and the copy is attached in Appendix 3 so the discussion in Chapter 3.2 is more focused on the comparison of DO3A-P^{ABn} and DO3A-P^{NBn}. Additionally, within this chapter, a rather peculiar

solid-state structure of the Y-DO3A-P^{ABn} complex is briefly presented (for the reprint of the full paper see the Appendix 4).

The Chapter 3.3 covers the work done on the ditopic system CS(DO3A-P$^{Bn(N)}$)$_2$ (Chart 2.1). This system was studied as a model for high-molecular conjugates of DO3A-P^{ABn} and also in respect to its potential application as CA. The solution study involves not only a classical multi-nuclear NMR characterization (^{1}H, ^{13}C, ^{31}P, ^{17}O) but also a quite rare ^{89}Y NMR spectroscopy. All details on this topic are presented in the paper just accepted for publication (Appendix 5.)

The final chapter (Chapter 3.4) includes the discussion of the results obtained on DO3A-P$^{Bn(N)}$ dendrimeric conjugates with PAMAM dendrimers of several generations (Chart 2.1). This work has been firstly published in the short communication (reprint in Appendix 6) and more details are presented in the full paper currently submitted (manuscript in Appendix 7). The discussion in the Chapter 3.4 is mainly focused on the most interesting topics in this subject, namely the interaction and the adduct formation of dendrimeric conjugates with polyaminoacids and pH-responsive behavior of these adducts.
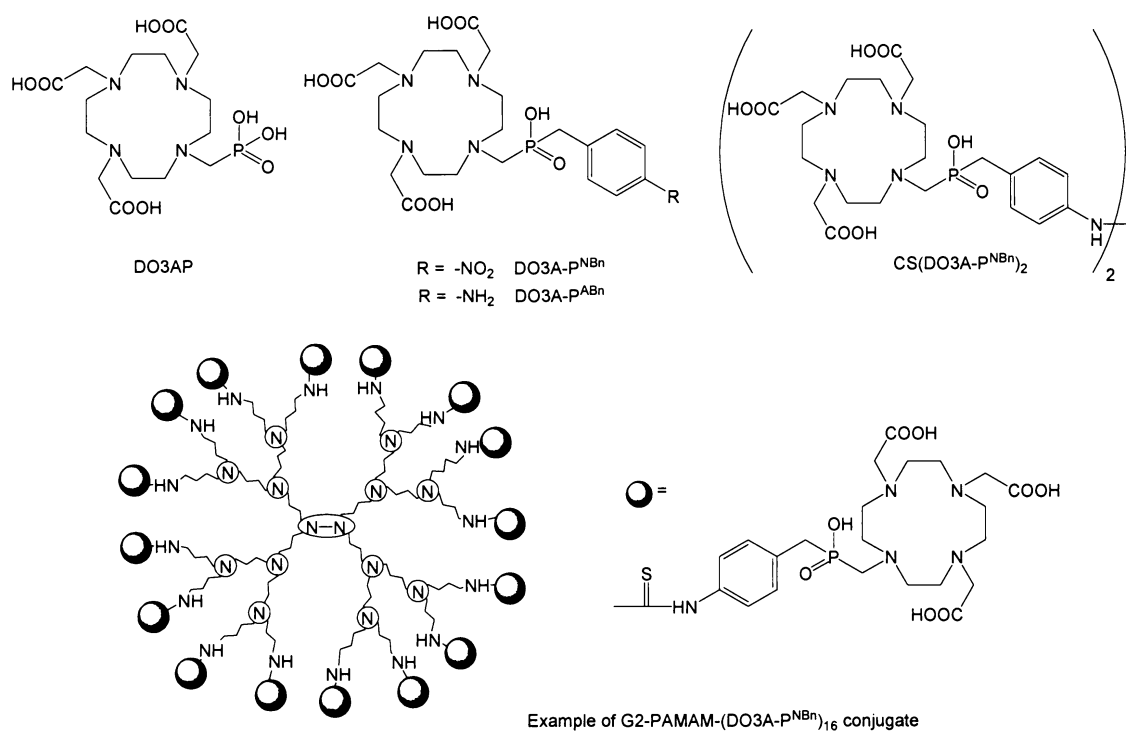

DO3AP

R = -NO$_2$ DO3A-P^{NBn}
R = -NH$_2$ DO3A-P^{ABn}

CS(DO3A-P^{NBn})$_2$

Example of G2-PAMAM-(DO3A-P^{NBn})$_{16}$ conjugate

Chart 2.1. The structures of the ligands studied in the Thesis.

3. Results and Discussion

3.1 DO3AP: Mono(methylphosphonate) Analogue of DOTA
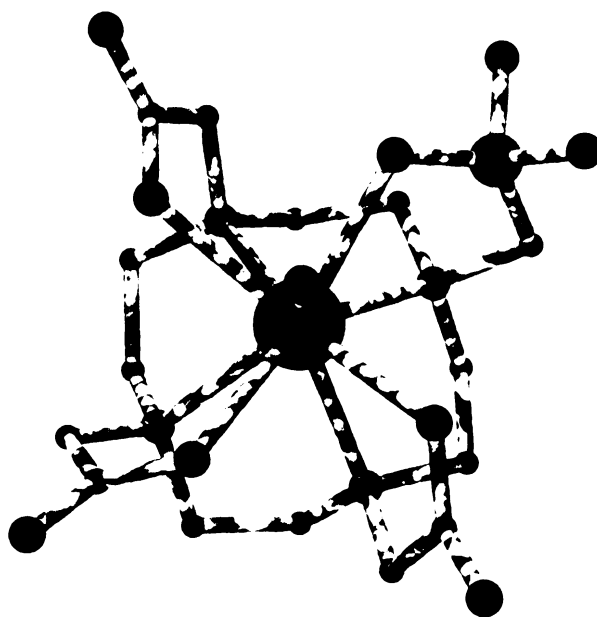
efore we got to design of the monophoshonate analogue of DOTA, several phosphorus-containing CA candidates were already known. From one part, they were DOTA-tetraphosphonates, tetraphosphinates and their various esters studied in detail by the groups of Parker, Sherry, Aime and our group.[63,65–67] It was found that the lanthanide(III) complexes of these ligands occur exclusively in more desirable TSAP-arrangement both in the solution and in the solid-state. The main drawback of these agents was the absence of coordinated water molecule in the first hydration shell, however, it was demonstrated that an extended second-hydration sphere might compensate that disadvantage. Another chelators explored by Aime *et al.* were the pyridine-containing phosphonate macrocyclic ligands as *e.g.* PCTP (see also Chart 1.2) designed for non-covalent conjugation to β-cyclodextrines.[80] The Gd-PCTP complex possess two coordinated water molecules and displays exceptionally short water residence lifetime ($^{298}\tau_M$ = 6 ns) in comparison with its tricarboxylate analogue (70 ns).[38] This was accounted for the higher steric demands of the phosphonate moieties. Combining all, the benefit from the second-hydration sphere, the higher abundance of the TSAP isomer and the fast water exchange rate, we decided to synthesize DO3AP (Chart 2.1) as a compromise structure.[81]The other aim

was to explore the influence of the pH on solution structural parameters because the pK_a corresponding to the protonation of the phosphonate moiety of the Gd-DO3AP complex is about 5.[81] In the first step, a coordination fashion of the new ligand was determined by a combination of a Dysprosium Induced ^{17}O NMR Shift measurement (DIS-^{17}O) and a separation of contact contribution to the Lanthanide Induced ^{17}O Shifts (LIS-^{17}O) (Figure 3.1a). Both these experiments indicated one capping water molecul along the lanthanide series. An octadenticity of DO3AP was complementarily proved by the shape of ^1H NMR spectra measured for Nd, Eu and Yb
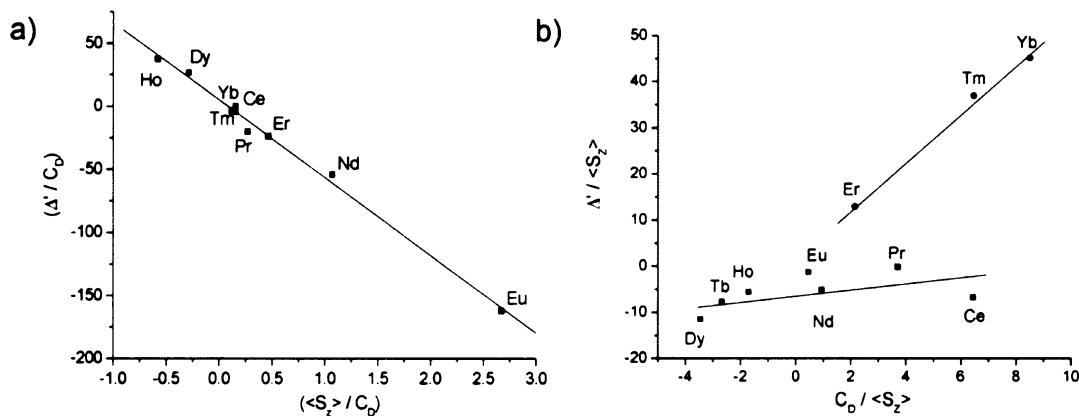

Figure 3.1. a) The separation of contact contributions to ^{17}O chemical shifts and b) the separation of pseudo-contact contribution to ^{31}P chemical shift of TSAP isomer of the Ln-DO3AP complexes. The color lines represent the alternative grouping of DO3AP Ln-complexes according to hydration manner (see the text) in comparison to that one presented in ref. [81]

complexes. Notably, whereas in the solid-state the Ln-DO3AP complexes showed exclusively TSAP structures[56,81], in the solution the mixtures of TSAP and SAP were found for lanthanides heavier then Nd(III).

In the next step, I intended to determine an abundance of the TSAP isomer along the lanthanide series. As it was not possible to measure ^1H spectra for all Ln-DO3AP complexes due to the unfavorable magnetic properties[28] of the heavier lanthanides, I used the phosphorus atom as a reporting nucleus. The TSAP/SAP isomeric ratio was also explored at variable pH. It appeared, that the most crucial issue would be an assignment of the ^{31}P NMR signals to isomeric species, especially for the heavier lanthanides(III) ions. To do that reliably, I measured the series of ^{31}P and ^1H spectra for different selected lanthanide(III) complexes at variable pH. Having assigned the ^{31}P resonances, it became clear that TSAP/SAP ratio changes significantly with pH (Figure 3.2) and, moreover, the TSAP abundance showed a completely different course along the lanthanide series than that reported for Ln-DOTA complexes. Importantly, the abundance of the TSAP isomer for Gd-DO3AP complex was found to be the same about 60% incidentally irrespective to the pH value; that is three-fold increase in respect to the parent Gd-DOTA complex. To explain the growing population of the TSAP isomer in acidic solutions, two explanations were pointed out:
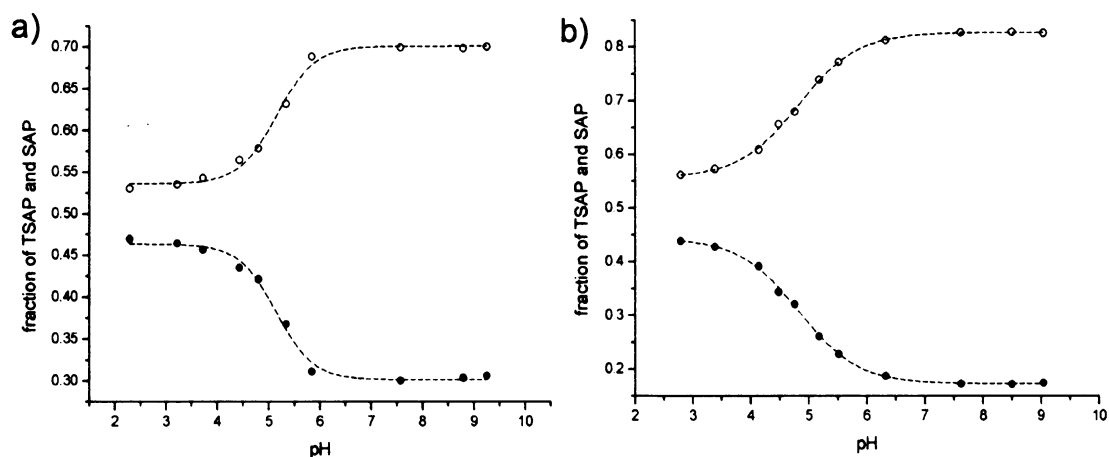
Figure 3.2. The molar fractions of TSAP (full circles) and SAP (open circles) as a function of pH for Eu (a) and Er (b) complexes of DO3AP. The dashed lines are sigmoidal fits to the experimental points for the determination of the pK_a values.

(i)   the electrostatic repulsion of the negative charges on the pendants in neutral and al-kaline pHs leads to a more expanded SAP structure whereas is acidic solutions more crowded TSAP structure is preferred.

(ii)   the highly ordered organization of the second-sphere hydration shell in acidic solu-tions somehow tends to prefer TSAP arrangement.

The later could be supported by the knowledge, that phosphonic and phosphinic acid moieties naturally preserve a certain number of water molecules aligned by a hydrogen-bonding network. It is also known that the extent of that network is strongly dependent on pH: in lower pH it is more extended due to a lower overall charge whereas the opposite is true for alkaline solutions. Additionally, the existence of the second-sphere was evidenced by the solid-state structure of the Nd(III) complex where two kinds of water molecules were found: one directly bound (Nd–O 2.5 Å) and the other in a close vicinity bound by hydrogen bonds at the Nd-O distance 2.6 Å.

As the next step, I made the plots of separated pseudo-contact contributions to the ^{31}P chemical shifts for SAP and TSAP isomers of all Ln-DO3AP complexes. Whereas the plot cor-responding to SAP isomer was linear for all complexes where this isomer occurs, in the later the trend was broken in the middle of the lanthanide series (Figure 3.1b). The explanation of this point claimed in the paper assuming the influence of different crystal-field parameters seems to be a less probable nowadays. The alternative explanation stems from the occurrence of a dehy-drated TSAP isomer (usually labeled TSAP') as the third isomeric species in the mixture. The existence of this isomer was supposed even before in the solutions of DOTA complexes with the heaviest lanthanides but only as a minor fraction.[54] In contrast, the comparison of ^{1}H spectra of Yb(III) complexes of DOTA and DO3AP reveals the TSAP' isomer is by far the major spe-cies in the solution of Yb-DO3AP: the overall integral intensities of TSAP and SAP ^{1}H reso-nances are 1:3 for DOTA and 9:1 for DO3AP (Figure 3.3). Noteworthy, we made the similar

observations later on the mono-phosphinate DOTA-like ligands and very recently on Ln(III) complexes of DO3AP monoethylester $(DO3AP^{OEt})$.[82] The consequent contradiction between isostructurality detected by ^{17}O and non-linearity of ^{31}P (TSAP) LIS could be explained by a relative insensitiveness of ^{17}O LIS experiment in respect to the complexes of the heaviest lanthanides like Er, Tm and Yb: the corresponding ^{17}O LIS values for these complexes are close to zero irrespectively to the hydration number (Figure 3.1a).

In spite of these controversies in the end of the lanthanide series, it should be emphasized that the q

Figure 3.3. The ^1H spectra of Yb(III) complexes of DOTA (a) and DO3AP (b) at 400 MHz, 25 °C and pH 7. The ^1H resonances of "H4" protons are marked.

= 1 was confirmed for Dy(III) (by DIS experiment)[81], Eu(III) and Tb(III) (by time-resolved luminescence)[83] complexes and, hence, it could be reliably assumed for the Gd-DO3AP complex.

In the second part of DO3AP study, I carried out a custom relaxometric characterization using variable-temperature (0–90 °C) ^{17}O transversal relaxation rates, R_2, at 400 MHz and ^1H NMRD profiles at 0.01–60 MHz (0.00024–1.5 T) at 25 °C and 37 °C. All these measurement were done at pH 2.5, 4.7 and 7. Interestingly, whereas the NMRD profiles were pH-independent, ^{17}O-profiles altered significantly with pH especially by passing from 4.7 to 7. In particular, the shape and the amplitude of the profiles were different for the protonated (pH 2.5 and 4.7) and the deprotonated complex species (pH 7). The simultaneous fitting based on BSM model of paramagnetic relaxation also indicated quite different values for water residence life-times τ_M: we obtained $^{298}\tau_M$ of 40 ns for pH 4.7, whereas 14 ns was found in the latter case (Table 3.1).

As is the case of TSAP/SAP ratio, I assume there could be two possible effects in the game (and/or both of them simultaneously):
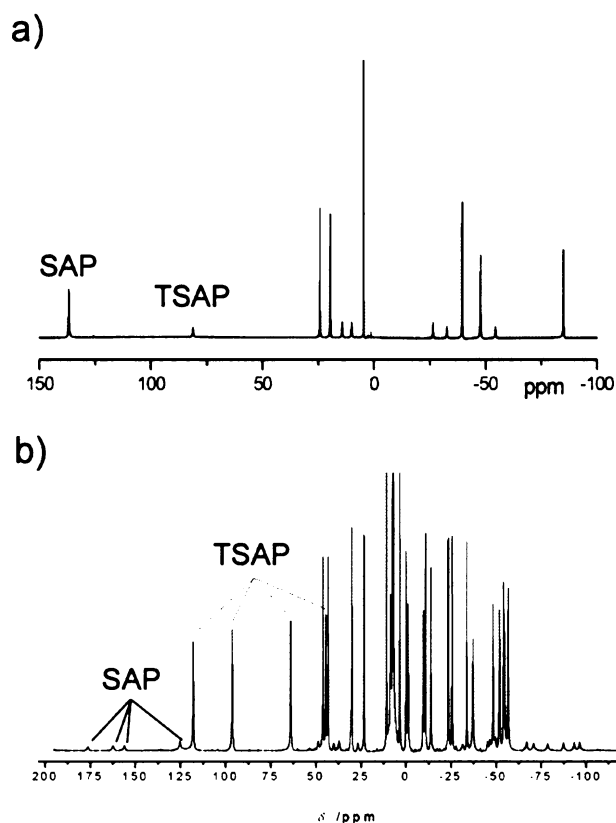
(i)   By the deprotonation, the water exchange process accelerates due to electrostatic repulsion between electronegative oxygen atom of the bound water and the negative charge predominantly located on the O4 plane of the complex.

.

(ii)   The second-sphere hydration shell is more organized in acidic solutions and, thus, holds the coordinated water stronger through the hydrogen bonds. Moreover, the entropy contribution to activation energy of dissociation should be higher. Both these factor results in elongation of the residence lifetime.

Table 3.1 Selected relaxometric parameters of systems discussed in the text and ref. [81] (Appendix 2)

Gd complex of	$^{298}\tau_M$ [ns]	$^{298}\tau_R$ [ps]	$^{298}\tau_v$ [ps]	$^{310}r_1{}^a$ [s^{-1} mM^{-1}]
DO3AP (pH 4.7)	40	70	3.3	4.11
DO3AP (pH 7.0)	14	83	3.9	4.57
DOTA	244	77	11	3.83

^{a} Milimolar relaxivity was measured at 37 °C and 20 MHz. ^{b} Ref. [84].

The first explanation is somewhat classical and has been supposed for Gd(III) complexes of macrocyclic DOTA-like ligands *i.e.* the systems with dissociatively activated water exchange.[85,86] The later one, more feasible in the case, was supported by several solid-state and solution studies on DOTA-derived tetra- and monoamides where the slow water exchange was observed irrespective to the overall charge of the complex (see ref. [81] and the references therein). The most recent support comes from the observations we recently made on the Gd(III) complex of tetrakis[hydroxomethylphoshonate]DOTP^{hm}. Despite no coorrdinated water molecule, we observed strong correlation between pH of the solution value and relaxivity that was ascribed to a pH-responsive organization of the second hydration sphere.[87] Generally, the water residence lifetimes found for the Gd-DO3AP complex at all pH values were quite short and stay within the optimal range predicted by BSM theory for imaging fields currently used in clinics (0.5-1.5 T).

In conclusion, DO3AP met our assumptions for its lanthanide(III) complexes keep a one coordinated water molecule (at least from La to Dy), the Gd(III) complex exchanges water molecule almost by one order of magnitude faster in comparison with the commercial agents and one may profit from the presence of the second-coordination sphere. The relaxivity of Gd-DO3AP is only moderately higher than that of Gd-DOTA but it should be emphasized that it is limited by the fast molecular tumbling as in the other low-molecular agents.[11] In order to fully benefit from the presence of the phosphorus acid pendant arm, it is necessary to conjugate the complex to a macromolecular carrier.

3.2 Ln(III) Complexes of Monophosphinate DOTA Derivatives
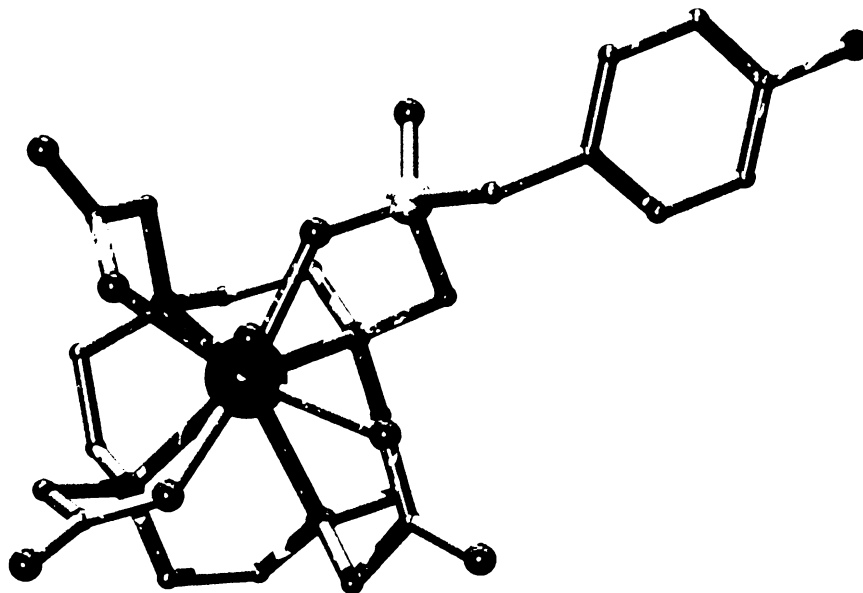
$\mathbf{I}$n progressing from "monomers" toward dendrimeric systems, the structure of DO3AP was modified by attaching a functionalized benzyl side-chain on the phosphorus atom. The goal was to prepare a Gd(III) complex endowed with a fast water exchange and ability to be covalently attached to a macromolecule via benzylthiourea moiety. In the previous chapter, it was briefly shown how the phosphonate might alter the properties of DOTA-like ligands. To investigate an effect of a phosphinate pendant on a structure and dynamics of Ln(III) complexes, I decided to focus on "monomeric" nitrobenzylderivative DO3A-P^{NBn} [88] and primordially aminobenzylderivative DO3A-P^{ABn} (Chart 2.1).[89]

The solution structure study was initiated by an assessment of a hydration number using a lanthanide-induced shift (LIS) measurement over the lanthanide series. In both systems, the ^{17}O LIS data exhibited linear trends indicating one coordinated water molecule. The caveats concerning the reliability of this outcome near the end of the lanthanide series were already mentioned in the case of DO3AP (Chapter 3.1). In order to surmise the structure of the Ln(III) complexes in solution, ^{1}H and particularly ^{31}P NMR spectra proved to be quite useful; ^{1}H spectra of Nd(III), Eu(III) and Yb(III) complexes confirmed an octadenticity of both ligands. In DO3A-P^{ABn}, its Eu(III) complex was the most intimately studied as europium flanks gadolinium in the lanthanide series and, thus, a close similarity of their structures could be expected. From the inspection of the ^{1}H and ^{31}P spectra (Figure 3.4a) of Eu-DO3A-P^{ABn} came out, that three iso-
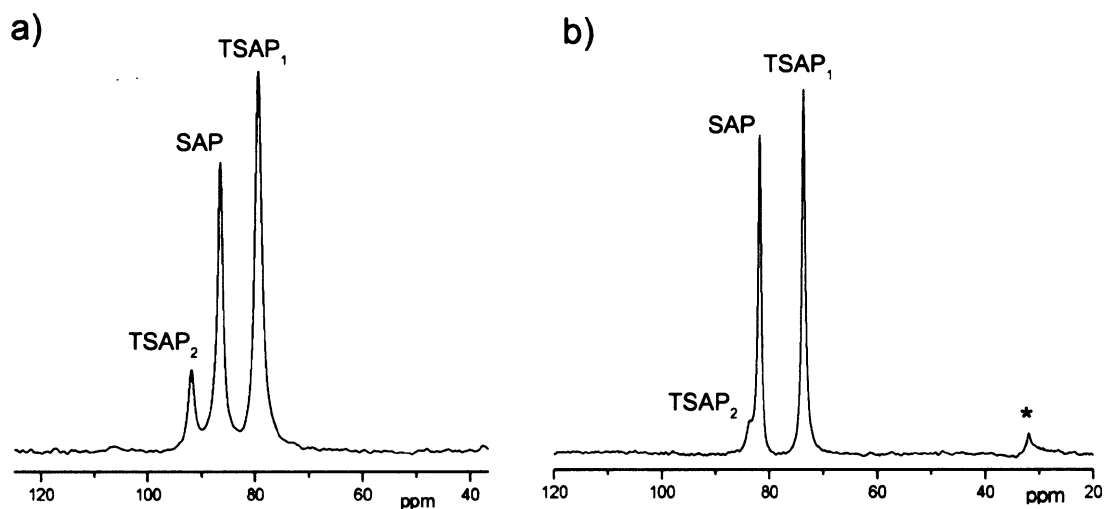
Figure 3.4. The ^{31}P NMR spectra of Eu(III) complexes of DO3A-P^{ABn} (a) and DO3A-P^{NBn} (b) at 161 MHz, pH 7 and 25 °C. The asterisk marks the signal of the free ligand.

meric species occur in solution instead of four possible diasteroisomers (Chapter 1.5). According to the chemical shifts and integral intensities, ^{1}H and ^{31}P resonances were assigned to TSAP$_{R(or\ S)}$, TSAP$_{S(or\ R)}$ and SAP isomers in respective ratio 1:5:4. The following study of the ^{31}P spectra at variable temperature (0–90 °C) revealed that the activation energy of the $R \leftrightarrow S$ interconversion is slightly higher than the SAP$\leftrightarrow$TSAP interconversion that was quantified by the determination of the coalescent temperatures. The occurrence of only three isomers was observed also for the other DO3A-P^{ABn} complexes. In addition, the NMR spectra of Ln-DO3A-P^{NBn} complexes were closely similar to those of DO3A-P^{ABn} except the abundance of the minor TSAP isomer was systematically bellow 10% (Figure 3.4b).[88] All these facts support the view that one arrangement of the phosphinate moiety is preferred over the other one and the missing SAP-type isomer simply does not exist instead of being in a fast dynamic equilibrium with its second SAP epimer on the phosphorus atom.

In respect to this point, quite recently we have studied in our group a system where a mono-ethylester phoshonate moiety (DO3AP^{OEt})[82] replaced the benzyl phosphinate. In the ^{31}P NMR spectra of Ln-DO3AP^{OEt}, all four possible isomers TSAP$_R$, TSAP$_S$, SAP$_R$ and SAP$_S$ were detected and, in the same time, R:S isomer ratios were not far from 1:1. The reason for such a striking dissimilarity between systems with the benzyl and the ethyloxo group is likely in much higher steric demands of the benzyl moiety. According to the molecular models based on the X-ray structures of the TSAP isomers of the Y-DO3A-P^{ABn} complex[90] (Figure 3.5), one orientation of the phosphinic moiety could be favored at a given rotation of pendant arms (Λ or Δ). The preference for a particular arrangement may arise from entropy reasons: in one arrangement, the rotation of the benzyl moiety is more or less free (R on Figure 3.5), whereas in the second one it is significantly hindered. Alternative explanation may be seen as much more speculative: I as-
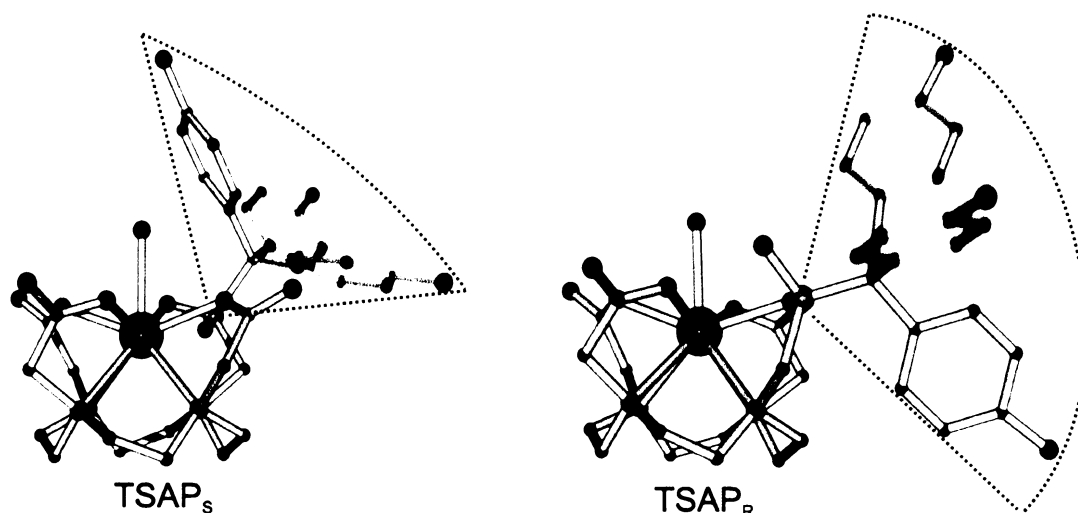
Figure 3.5. The molecular models based on the solid-state structure of the Y-DO3A-P^{ABn} complex. Gyration motion of the benzyl group is indicated by there arrangements rotated mutually by 120° around the $P-CH_2(-Bn)$ bond.

sume that Ln-DO3A-P^{ABn} complexes prefer the isomer, where the aminobenzyl moiety could participate in the second-sphere hydrogen bonding through its amino group. On the other hand, in Ln-DO3A-P^{NBn}, the hydrophobic nitrobenzyl group would be located preferably aside the hydrophilic O4 (see also below). In order to explain the absence of the second SAP isomer, it is worth to note that the SAP wrapping is more rigid and compact in comparison to TSAP[56,90] and, in turn, one arrangement could be exclusively preferred.
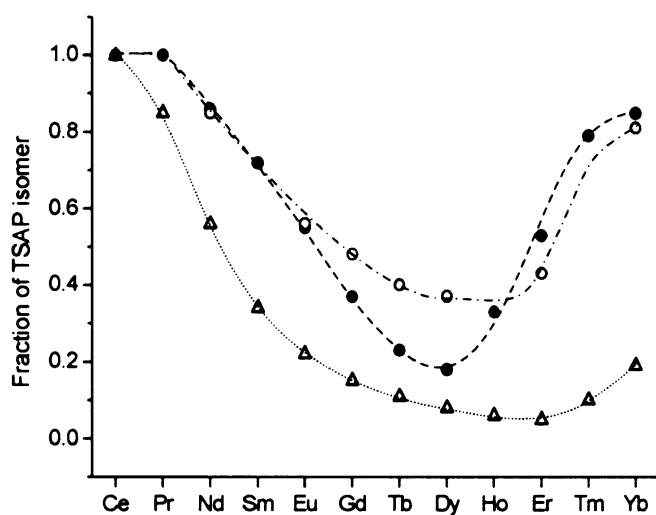
Figure 3.6. The profiles of TSAP abundance for Ln(III) complexes of DO3A-P^{ABn} (full circles), DO3A-P^{NBn} (open circles) and DOTA (open triangles). The corresponding ^{31}P NMR spectra were measured at pH 7 and 25 °C. The red points are the values for the Gd(III) complexes obtained by an interpolation. The lines are just to guide the eyes.

The abundances of the TSAP isomer for both phosphinates differ dramatically from that of DOTA (Figure 3.6) and conversely, they parallel the Ln-DO3AP series. The TSAP$_{R,S}$ fractions are about 40% for the Gd(III) complex; it is doubled in comparison with Gd-DOTA. The Yb(III) complexes showed 80% abundance of TSAP$_{R,S}$. Likewise, the explanation stems from the existence of the dehydrated TSAP' isomer in complexes with heavy lanthanides, however, the equilibrium be-

tween these three isomers has been recently indirectly proved as all three forms were curiously found in one single-crystal of the Y-DO3A-P^{ABn} complex (Figure 3.7).[90]
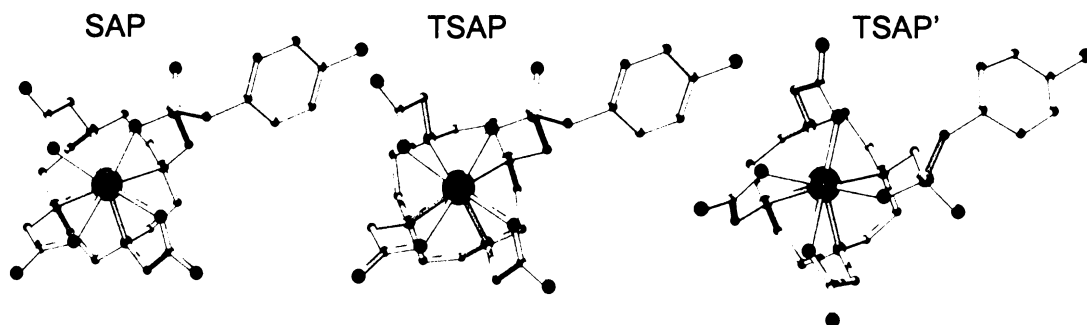
Figure 3.7. The drawings of the three independent complex units found in the single-crystal structure of the Y-DO3A-P^{ABn} complex. The pictures are based on the real parameters; only hydrogen atoms and thermal ellipsoids are omitted for the clarity.

It is notable, that the hydration TSAP isomers could not be detected by either ^{1}H or ^{31}P NMR spectra of the studied systems as the water exchange rate is by several orders of magnitude faster than the timescale of the NMR measurements. In addition, the TSAP$_R$:TSAP$_S$ ratio seems to be almost the same along the whole lanthanide series; so, both the hydration and the wraping isomerisms are effectively independent. Exactly the same situation was observed for the Ln-DO3AP^{OEt} complexes.[82]

Having all necessary structural information, I proceeded with the custom relaxometric characterization of the Gd(III) complexes using VT-^{17}O NMR and ^{1}H NMRD measurements. The experimental data were then simultaneously evaluated on the basis of BSM relaxation model. As a rather high number of parameters was engaged, several of them were fixed to custom or independently obtained values. The complete results for the complexes of both ligands are comprised in Table 3.2.

Despite the structural similarity between the ligands, a mere qualitative comparison of both systems in terms of their ^{17}O-R_2 and ^{1}H NMRD profiles revealed several major differences (Figure 3.8). Consequently, the numerical evaluation indicated rather different dynamic properties of the Gd-DO3A-P^{ABn} and Gd-DO3A-P^{NBn} complexes. The water residence lifetime grew up more than three times by going from the amino- to the nitroderivative. A qualitatively similar effect was observed for amino- and nitrophenyl derivative of DO3A where the water residence lifetime increased by factor of 2.3 with a substitution of amino- with nitro- group on the phenyl ring.[91] The authors explained the observation by assuming both phenyl moieties to have different nature of an induction effect on a coordinated nitrogen atom.[91] However, this explanation seems to be less likely for the phosphinates. The reorientational motion of Gd-DO3A-P^{NBn} was slowed down by 50% in respect to Gd-DO3A-P^{ABn} that was responsible for a 20% increase of the relaxivity. Moreover, to obtain a meaningful fit, it was necessary to fix two water molecules,

Table 3.2. The results from the simultaneous fitting of ^{1}H NMRD and VT-^{17}O NMR R_{2r} data for Gd(III) complexes of DO3A-P^{ABn} and DO3A-P^{NBn}.

Parameter	ligand	
	DO3A-P^{ABn} [a]	DO3A-P^{NBn} [b]
$^{310}r_1$ [s^{-1} mM^{-1}] [c]	5	6.2
Δ^2 [10^{20} s^{-2}]	0.25 ± 0.01	0.77 ± 0.02
$^{298}\tau_M$ [ns]	16.2 ± 0.1	52 ± 1
ΔH_M [kJ mol^{-1}]	20.6 ± 0.3	61.5 ± 0.7
$^{298}\tau_R$ [ps]	88 ± 4	137 ± 4
E_r [kJ]	29 ± 1	37 ± 2
$^{298}\tau_v$ [ps]	11.2 ± 0.1	6 ± 0.1
$A/\hbar$ [10^6 rad s^{-1}] [d]	$\underline{-2.89}$	$\underline{-2.48}$
R_{GdO} [Å]	$\underline{2.6}$	$\underline{2.5}$
R_{GdH} [Å]	$\underline{3.1}$	$\underline{3.1}$
A [Å]	$\underline{3.6}$	$\underline{3.5}$
ΔH_{mss} [kJ]	$\underline{15}$	$\underline{15}$
$^{298}\tau_{rss}$ [ps]	9 ± 2	20 ± 2
R_{ss} [Å]	$\underline{3.6}$	$\underline{3.5}$
$^{298}\tau_{mss}$ [ns]	$\underline{1}$	$\underline{1}$
q	$\underline{1}$	$\underline{1}$
q_{ss}	$\underline{1}$	$\underline{2}$

[a] ref [89]; [b] ref [88]; [c] at 37 °C and 20 MHz; [d] The values of the hyperfine coupling constants were calculated from ^{17}O LIS. The underlined values were fixed during the fitting. The value of E_v was fixed to 1 kJ. The meaning of all parameters are explained in Appendix 1.

q_{ss} = 2, in the second sphere of the Gd-DO3A-P^{NBn} complex in contrast to one water molecule in the Gd-DO3A-P^{ABn} complex. Likely, these differences could be explained by considering a different polarity of benzyl moieties; aminobenzyl group (pK is 5.48[92]) should be rather hydrophilic at a neutral pH (pH=7) in contrast to the hydrophobic nitrobenzyl group. It might be assumed that the aminobenzyl is in a close contact with the second-sphere water molecules producing a more compressed structure, whereas the nitrobenzyl side chain lingers aside. In turn, the nitrobenzyl structure is more relaxed diminishing the water exchange, but on the other hand, effective molecular size is effectively larger.

In summary, gadolinium(III) complexes of the monophosphinate DOTA analogues exhibit quite promising properties for an attachment to a macromolecule; the water exchange proved to be sufficiently fast and even close to the optimal range. The overall relaxivity is higher up to 30% in comparison to Gd-DOTA likely owning to the slower molecular tumbling and the contribution of the second hydration sphere. Comparing Gd-DO3A-P^{ABn} and Gd-DO3A-P^{NBn} com-

plexes, it was demonstrated that even a quite subtle change of a ligand structure may noticeably alter the chelate dynamics.

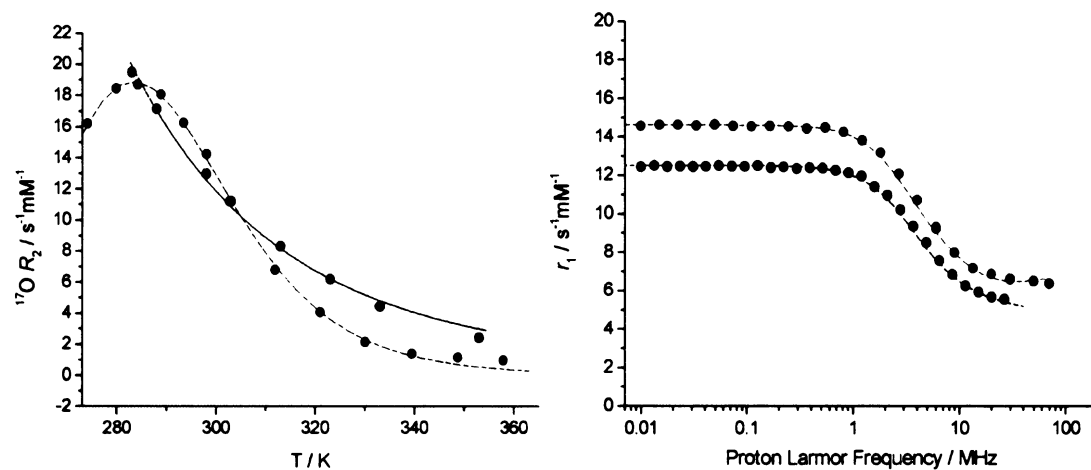**Figure 3.8.** The comparison of VT-^{17}O relaxation rates R_2 (left) and ^{1}H NMRD profiles at 25 °C (right) for Gd-DO3A-P^{ABn} (black) and Gd-DO3A-P^{NBn} (red). The lines represent the best fit to the experimental data. The ^{17}O temperature profile of Gd-DO3A-P^{NBn} was measured at 54 MHz whereas that one of Gd-DO3A-P^{ABn} at 68 MHz. All experiments were carried out at pH 7.
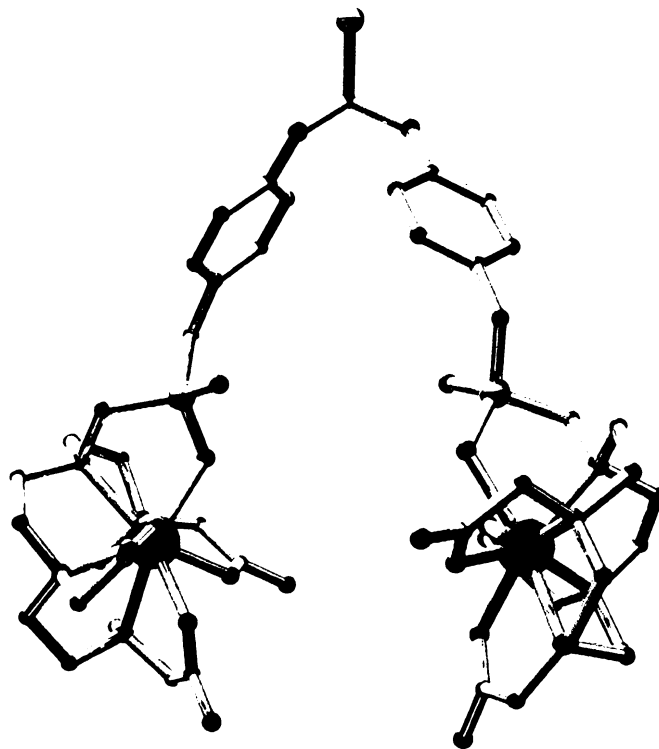
imeric and multimeric structures are on halfway between monomeric and macromolecular contrast agents. This class of compounds has been studied for more than decade as they represent a relatively simple way how to prepare candidates with a longer rotational correlation time and, in turn, a higher relaxivity. In addition, the multimeric structures with higher "concentration" of gadolinium in a molecule exhibit a higher relaxivity per mass unit (r_{eff}); it means that lower injection volumes could be administered to reach the same dose of Gd per kg of body-weight. Among the multimers that have been te most frequently studied are dimeric structures based on symmetrical DOTA-like chelating units linked by various types bridges (Chart 3.1).[93-97] Unfortunately, most of them displayed an undesirably low water exchange rate inherited from the parent DOTA monomer and also their relaxivities were hampered by a high flexibility of the linking moiety. In the last two years, a nice examples of the fast-exchanging and rather rigid multimetal systems have appeared,[98] however, their metallostar structures based on heptacoordinated Gd(III) units would critically limit a kinetic stability for *in vivo* applications. In the light of these facts it still seems desirable to continue designing structures endowed with a fast water exchange, high segmental rigidity and sufficient stability in order to benefit from the concept of multimers.
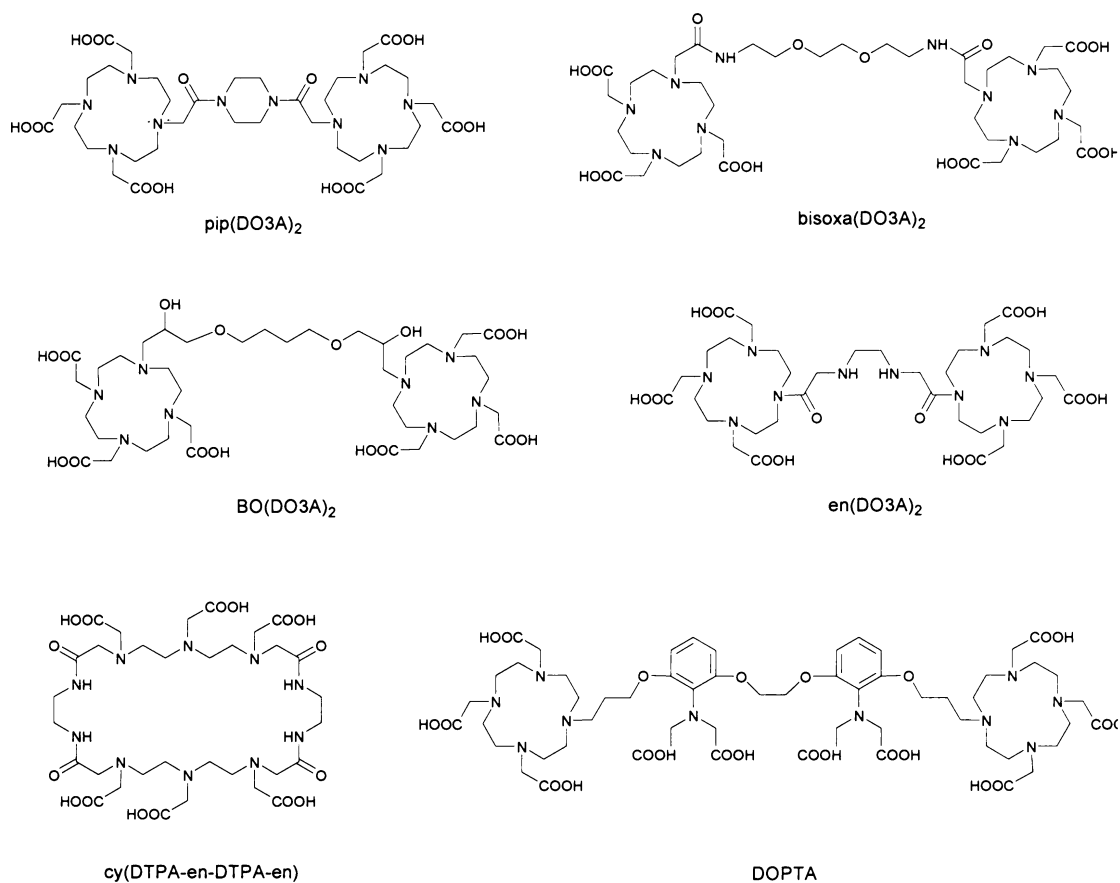
Chart 3.1. The structures of selected dimeric ligands.

Bearing in mind the convenient properties of the phosphinate ligands mentioned before (Chapter 3.2), I prepared the ditopic chelator joining two monophosphinated $DO3A-P^{ABn}$ units by a thiourea linker (Chart 2.1).[99] This linking group was chosen deliberately to get not only a worthy candidate for CA but also to prepare a model compound for thiourea-conjugated dendrimers. The solution structural study, preceding a relaxometric evaluation, was originally limited only to an investigation of the Eu(III)/Eu(III) complex. Its ^{1}H NMR spectra seemed to be characteristic for a C_1-nonsymmetrical chelating macrocyclic unit and perfectly matched those of its monomeric $Eu-DO3A-P^{ABn}$ and $Eu-DO3A-P^{NBn}$ homologues (Figure 3.9). On the contrary, in the ^{31}P NMR spectrum of the dimeric complex, 10 resonances were found about at 25 °C (Figure 3.9) and even more at lower temperature.

The most likely, the shape of the ^{31}P NMR spectra results from the interplay of isomerism of both independent chelate units; both units may adopt four arrangements, $TSAP_R$, $TSAP_S$, SAP_R, SAP_S, and combining them independently into pairs, there is possible to have 10 distinct diastereoisomers giving rise to 16 ^{31}P resonances. The reason why the ^{1}H NMR spectroscopy does not reflect that feature can be explained by a dramatically different sensitivity of the phosphorus atom and hydrogen atoms. The phosphorus atom is the center of the *R/S* chirality and it
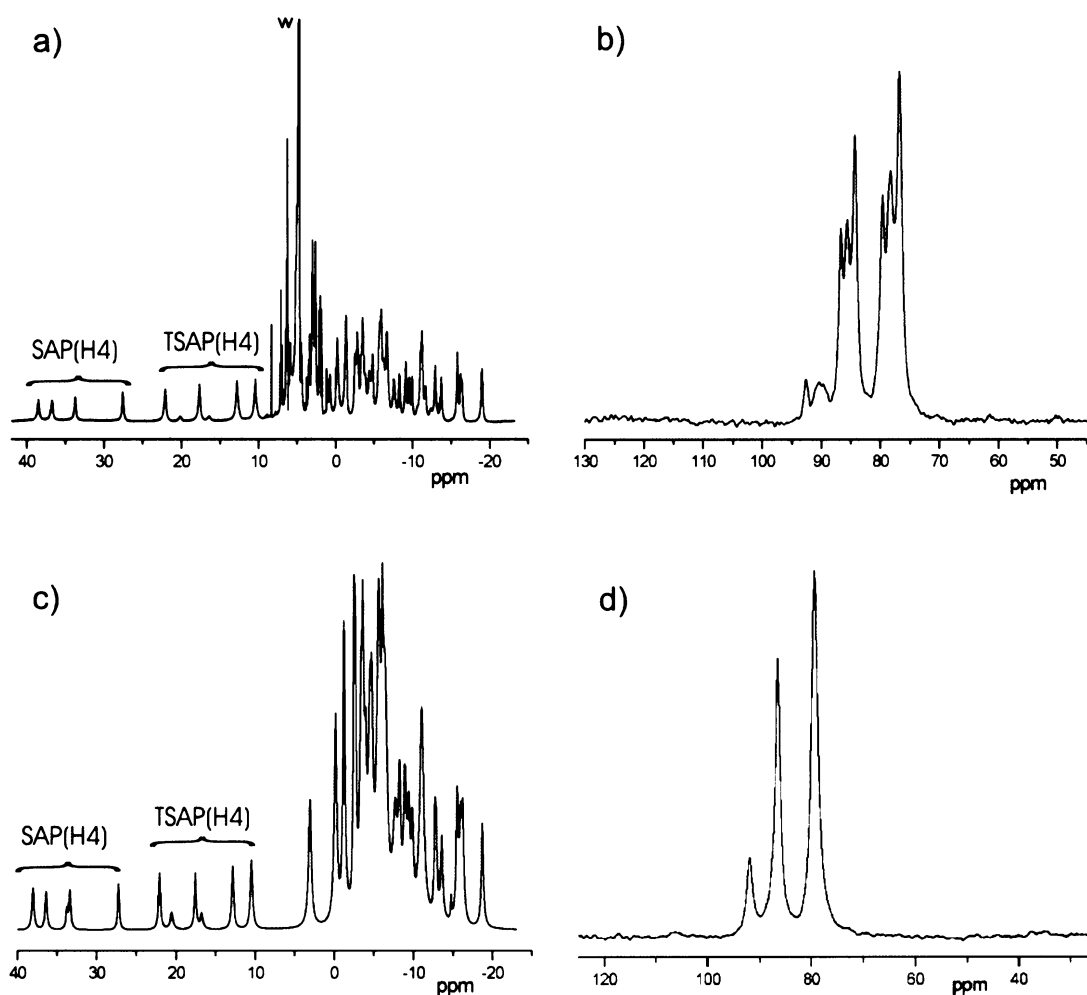
Figure 3.9. The comparison of ^{1}H and ^{31}P NMR spectra of the Eu-DO3A-P^{ABn} and Eu$_2$-CS(DO3A-P$^{Bn(N)}$)$_2$ complexes: ^{1}H spectrum (a) and ^{31}P spectrum (b) of Eu$_2$-CS(DO3A-P$^{Bn(N)}$)$_2$; ^{1}H spectrum and (c) and ^{31}P spectrum (d) of Eu-DO3A-P^{ABn}. All spectra were measured at 400 MHz (^{1}H), pH 7 and 25 °C.

is also involved in the linking. On the other hand, the most shifted protons (H4) are unaffected as they are on the ring backbone.

Rather important issue was to determine the shape of the complex in solution; in particular, to assess whether it is oblong or spherical, as this would have a great impact on dynamics of the complexes. In order to estimate the mutual distance of the chelate subunits, the mixed Y(III)/Gd(III) complex (and also the bis-Y(III) one) was synthesized. From the measurement of T_1 relaxation times of ^{13}C and ^{89}Y, we were able to calculate average distances between Gd(III) ion and the reporting nuclei. In contrast to what was expected, the metal-metal distance seemed to be quite short (6.25 Å) and both units arranged in a face-to-face manner. An average distance between the Gd(III) ion and the ring carbons was equal to 8.2 Å that strongly supported this finding. According to a molecular modeling, we obtained a rather compact structure where both units are hold in a close contact, which nevertheless allow water molecules to diffuse in and out

freely. Unfortunately, up to now, I was not able to obtain a single crystal of an X-ray quality to prove these observations also in the solid state.

Performing the relaxometric evaluation based VT-^{17}O NMR and ^{1}H NMRD measurements, I firstly compared the data of the bis-Gd(III) and Gd(III)/Y(III) complexes in order to confirm or exclude an undesired influence of an electronic dipole-dipole interaction between the metal centers. Since both the ^{1}H NMRD and the ^{17}O profiles differed less than by 5%, I used the well established BSM approach for the quantitative evaluation of the bis-Gd(III) complex (Table 3.3).

**Table 3.3**. The values of the discussed relaxometric parameters for selected dimeric ligands.

Gd complexes of	[a] r_1 [s^{-1} mM^{-1}]	$^{298}\tau_M$ [ns]	$^{298}\tau_R$ [ps]	$^{298}\tau_v$ [ps]	q	ref.
CS(DO3A-P$^{Bn(N)}$)$_2$	6.1	53	183	16	1	99
pip(DO3A)$_2$	5.8	670	171	19	1	93
bisoxa(DO3A)$_2$	4.9	714	106	15	1	93
BO(DO3A)$_2$	4.6	1000	250	NA	1	94
en(DO3A)$_2$	3.6	769	105	17	1	96
cy(DTPA-en-DTPA-en)	4.8[b]	3448	188	21	1	95
DOPTA	3.3[c]	NA	NA	NA	1	97

[a] value are given at 37 °C and 20 MHz; [b] the value was estimated from the chart; [c] the authors did not state conditions; NA – not available.

Comparing the results for the dimer with the parent monomeric complex Gd-DO3A-P^{ABn}, there are two notable features: (i) the rotational correlation time grew up just about twice and (ii) the water residence lifetime decreased more than three times (but still remain close to the optimal value). Doubled $^{298}\tau_R$ with the two-fold increase of the molecular weight supports the model of a compact structure lacking a substantial degree of the internal flexibility. In contrast, the decrease of water exchange rate from 16 ns to 53 ns perfectly parallels the effect observed in the Gd(III) complexes of DO3A-P^{ABn} and DO3A-P^{NBn} monomers ($^{298}\tau_M$ = 52 ns). Likewise, this could be ascribed to a different polarity of the benzyl moiety with the change of the substituent or, alternatively, the compactness of the ditopic structure may after all slightly hinder the water exchange. By itemizing the overall relaxivity of the ditopic and the parent monomeric complexes to particular contributions, it is apparent that the inner-sphere and the second-sphere terms are doubled for the ditopic complex whereas the outer-sphere contribution remained unchanged. In result, the overall relaxivity of the dimer was increased by factor of 1.5 in comparison with that of parent Gd-DO3A-P^{ABn} complex.

It is worth to note, that the relaxivity 6.1 s^{-1}mM^{-1} (37 °C and 20 MHz) of Gd-CS(DO3A-P$^{Bn(N)}$)$_2$ is, to my best knowledge, the highest value for any dinuclear complex with q = 1 reported so far but, of course, further increase of the molecular weight will be necessary to attain really high efficacies.

3.4 PAMAM Dendrimeric Conjugates with DO3A-P$^{Bn(N)}$ Chelating Unit
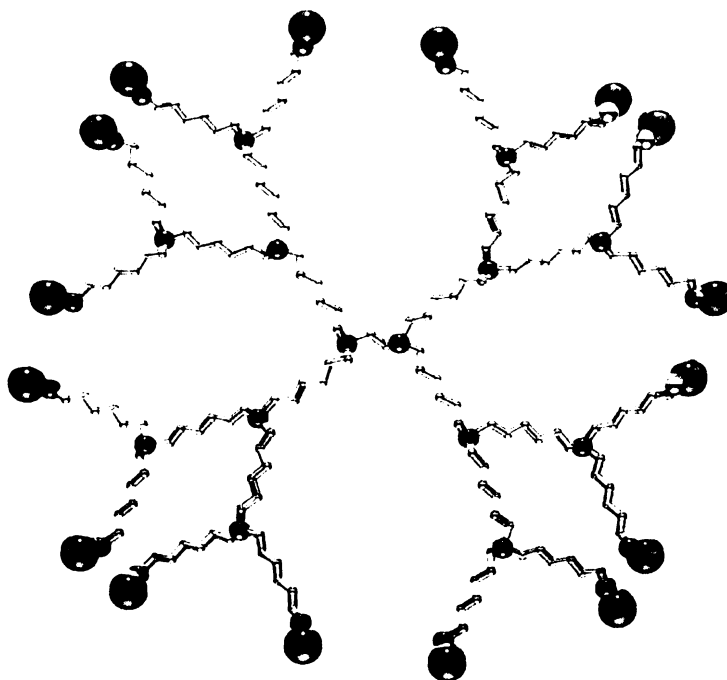
aving the information about the solution structure and dynamics of the monomeric and the ditopic phosphorus-containing systems, I came to the preparation and investigation of dendrimeric conjugates. As the carriers, starburst polyamidoamine dendrimers (or shortly PAMAMs) were chosen. These dendritic macromolecules have been extensively studied for last 20 year for their broadly favorable properties; they are commercially available in a variety of generations (G1-G11) and core-types, their structural properties have been largely explored.[100] Their syntheses have been handled in a way to offer almost monodispersive products on kg-scale. For their low-toxicity and high water solubility, a significant progress has been made toward the application of PAMAM-based structures as drug-delivery vectors, for a gene therapy and/or in immunodiagnostics.[76] In the last decade, PAMAMs have been also exploited in the field of CAs as building blocks for covalent conjugates. The most explored systems are conjugates with DTPA[101] and DOTA-like[102] chelators in a wide range of sizes (generations 2-9). Unfortunately, these conjugates were not evaluated in-depth from the relaxometric point of view but mostly in respect to their potential clinical applications.[101,102] Nevertheless, their efficacies are known to be limited by a slow water exchange and high flexibility of their structures.[11] Recently, PAMAM conjugates with a fast-exchanging Gd-EPTPA (EPTPA = ethylene-propylentriaminepentaacetic acid) chelate were reported[103] but the undesired internal motion
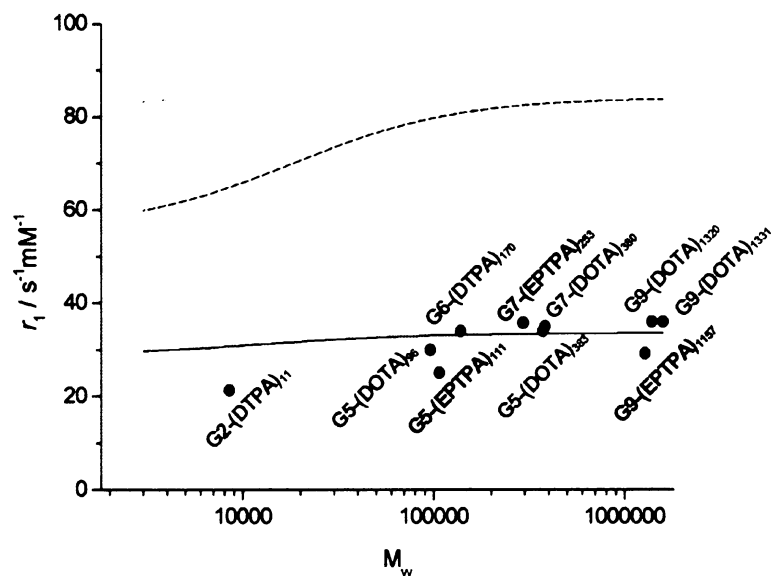
Figure 3.10. The plot of relaxivity as a function of a molecular weight for selected PAMAM-conjugated systems. The lines are simulations of relaxivity at 20 °C and 20 MHz for $^{298}\tau_M$ set to 300 ns (solid line) and 6 ns (dashed line) assuming the conjugates as totally rigid spheres. The values of the other parameters involved in BSM model were following: τ_v = 30 ps, Δ^2 = 0.1×10^{20} s^{-2}, q = 1, R_{GdH} = 3.1 Å and a = 3.5 Å. The molecular tumbling times, τ_R, were calculated using Debye-Stokes equation. Molecular radii of PAMAM conjugates needed for this calculation were estimated on the basis of the correlation function between the molecular weights and gyration radii of free PAMAMs determined by SASC measurement (adopted from ref. 100).

still remains non-addressed. The effect of a the low water exchange rate and the lack of segmental rigidity are demonstrated on Figure 3.10 where the experimental relaxivities for the selected slow-exchanging (DOTA and DTPA, $^{298}\tau_M \sim$ 300 ns) and fast-exchanging (EP-TPA, $^{298}\tau_M \sim$ 6 ns) PAMAM conjugates are plotted against their molecular weights. In the comparison, there are also shown the simulated dependences of relaxivity on M_w for two values of water residence lifetime, $^{298}\tau_M$ = 300 and 6 ns. In the simulations, conjugates were assumed as totally rigid spheres. Apparently, the relaxivities of rather different systems are quite similar, independent of their water exchange rates unless the internal flexibility is "frozen".

For my study, I chose lower generation PAMAMs with an ethylenediamine (EDA) core, namely, G1-, G2- and G4-generations exposing 8, 16 and 64 primary amines on their surfaces free for a thiourea conjugation. An advantage in choosing the low-molecular dendrimers stems from a good accessibility of their surfaces toward the conjugation with a bifunctional chelate giving rise to almost quantitative yields in comparison to a typical ~50% yield in their high-generation homologues.[101–103] Moreover, low-molecular conjugates and their complexes could be more easily characterized by methods of organic chemistry and a comparison with their monomeric precursors is more straightforward. I prepared four conjugate species: except "fully-saturated" G1-(Gd-DO3A-P^{NBn})$_8$, G2-(Gd-DO3A-P^{NBn})$_{16}$ and G4-(Gd-DO3A-P^{NBn})$_{59}$ also the "half-saturated" G2-(DO3A-P^{NBn})$_9$. A full structural characterization was done by means of ICP-MS, ^{1}H NMR, elemental analyses and by relaxometric titrations.

The first issue I was focused on was the dependence of relaxivity on pH. Formerly, it was known, that PAMAMs as polyelectrolytes change their solution conformation in dependence on
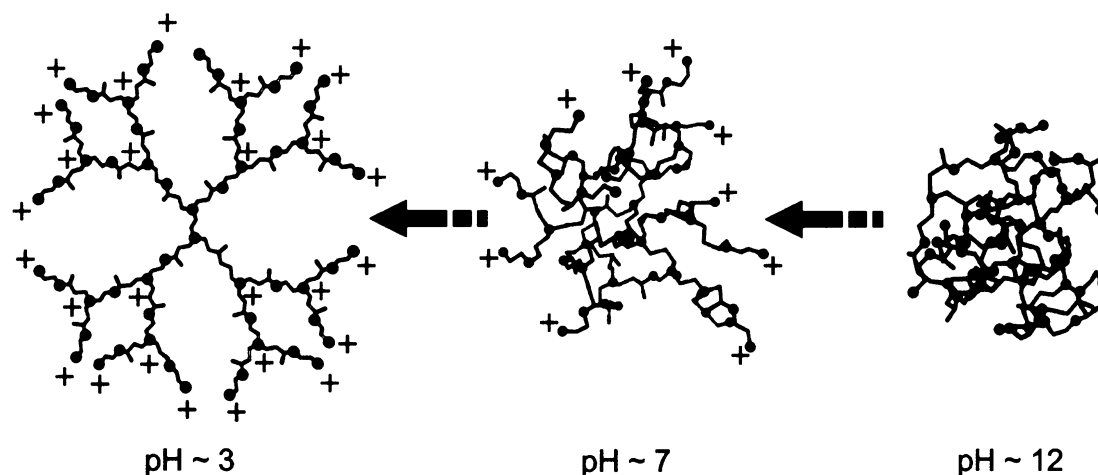
Figure 3.11. The schematic drawing of the structural pH-responsive behaviour of the G2-PAMAM dendrimer.

a protonation degree: as the positive charge grows in acidic media, the structure tends to be more spread-out due to an electrostatic repulsion (Figure 3.11).[104] This process is projected also into the values of relaxivity as was independently explored in PAMAM-based CAs by Merbach *at al.*[103] and by our group.[105,106] The dependencies of relaxivity on pH for all prepared DO3A-P^{NBn}-based dendrimeric Gd(III) complexes showed a quite significant step at pH ~5.5 (Figure 3.12a). In addition, the comparison of the ^{1}H NMRD profiles at pH 7 and 4 revealed that by passing from neutral to acidic solutions, the molecular tumbling was slowed down.[106]

To get more insight, I carried out the NMR titration of a pure G2-PAMAM dendrimer (Figure 3.12b). Except the increase at pH ~9 corresponding to the protonation of primary amines, the second step was detected at a quite similar pH value as it was found for the conjugates. The connection between these observations signifies that, by the protonation of the PAMAM backbone, the effective molecular size increases and, in turn, the relaxivity grows up for 10 to 30%. The differences in the shapes of the pH profiles were ascribed to a different structural density and flexibility of the PAMAM structures. In the next stage, the relaxometric characterization based on ^{1}H NMRD and VT-^{17}O NMR was done. From a qualitative inspection, it was clear that the relaxivity is controlled by a molecular motion: ^{17}O R_2 profiles showed the maxima at a low temperature and the ^{1}H NMRD profiles were downscaled with a rising temperature (Figure 3.13).

For the simultaneous evaluation of the data, the more complex Lipari-Szabo[107] approach taking into account two distinct motional processes was used: except the global reorientation of the whole conjugate, there is a number local motions like a chelate rotation or a segmental motion of the dendrimeric backbone. Moreover, in order to achieve a meaningful fit, it was necessary to include a second-sphere contribution into the model. The results from the simultaneous fitting are comprised in Table 3.3 in comparison with the selected macromolecular systems. In

43
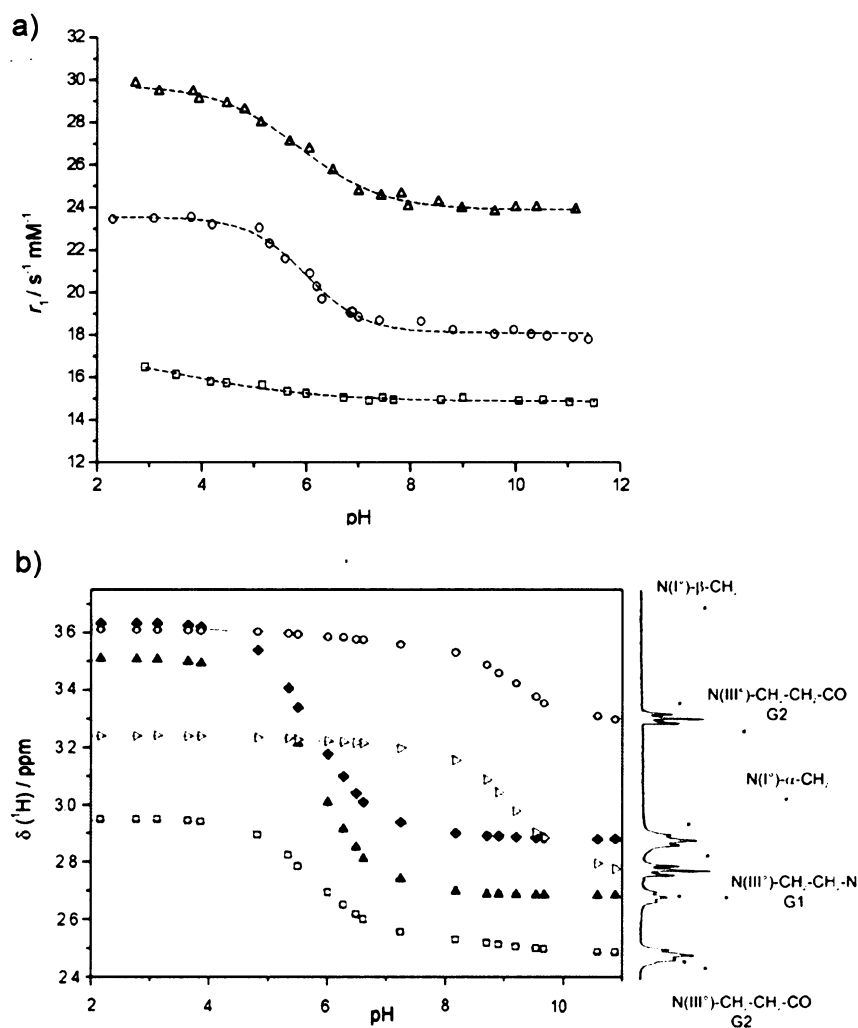
Figure 3.12. The relaxivity as a function of pH for the studied conjugates at 20 MHz and 25 °C: ascendantly from G1-8 to G4-64 conjugate (a). The dashed lines are just to guide the eyes. The ^{1}H NMR titration of pure G2-PAMAM conjugate at 400 MHz and 25 °C (b). The solid lines are the result of the simultaneous fitting. The trace shown on the right side is the corresponding part of the proton spectrum with the assignment.

accord with an expectations, the water residence lifetime, $^{298}\tau_M$, was elongated from 16 ns for the parent Gd-DO3A-P^{ABn} complex to 50–70 ns for the conjugates. This diminution of the water exchange rate could be accounted for an increased complexity of the structure but noteworthy it is far from being a relaxivity-limiting factor. Conversely, the critical parameter in this context seems to be a Lipari-Szabo rigidity term S^2 varying generally from 1 for totally rigid molecules to 0 for totally flexible ones.[107] For studied DO3A-P^{NBn} conjugate, it was about 0.25 (Table 3.3) signifying rather flexible structure and, consequently, the relaxivities of the studied conjugates are only moderate in comparison with the theoretical values. In fact, this outcome is somewhat

Table 3.3. The comparison of water residence lifetimes, rotational corelation times and relaxivites for the studied conjugates, selected macromolecular systems analyzed by the Lipari-Szabo approach. The data for parent the monomeric Gd-DO3A-P^{ABn} and the Gd$_2$-CS(DO3A-P$^{Bn(N)}$)$_2$ complexes were included.

Gd-complex of	$^{310}r_1$ [s^{-1}mM^{-1}]	$^{298}\tau_M$ [ns]	$^{298}\tau_{rg}$ [ps]	$^{298}\tau_{rl}$ [ps]	S^2	Ref.
dendrimers						
G1-(DO3A-P^{NBn})$_8$	10.1	48	1560	115	0.25	106
G2-(DO3A-P^{NBn})$_{16}$	14.1	66	2690	100	0.24	106
G4-(DO3A-P^{NBn})$_{59}$	18.6	68	3140	133	0.29	106
G5-(EPTPA)$_{111}$[a]	13.7	6	2950	125	0.36	103
G5(N{CS}N-Bz-DO3A)$_{52}$	18.7	NV	870	NA	NA	52
G6(N{CS}N-Bz-DTPA)$_{170}$	34	NV	NV	NV	NV	101
Gadomer 17 [b]	17.2	1000	3035	760	0.50	51
non-covalent conjugates						
G2-(DO3A-P^{NBn})$_{16}$–poly(Arg)$_{56}$	30.8	97	3890	172	0.35	106
DOTA(BOM)$_3$–HAS	53.2	80	NV	NV	NV	108
MS-325–HAS	48.9	NV	3000-4000	NA	NA	50
monomer and dimer						
CS(DO3A-P$^{Bn(N)}$)$_2$	6.2	53	NA	183	NA	99
DO3A-P^{ABn}	5	16	NA	88	NA	89

[a] measured at pH 9.9; [b] synthetic dendrimer based on polylysine structure with the DOTA-monoamide unit; NA = not applied; NV = not avaliable. The meanings of all parameters are explained in Appendix 1.
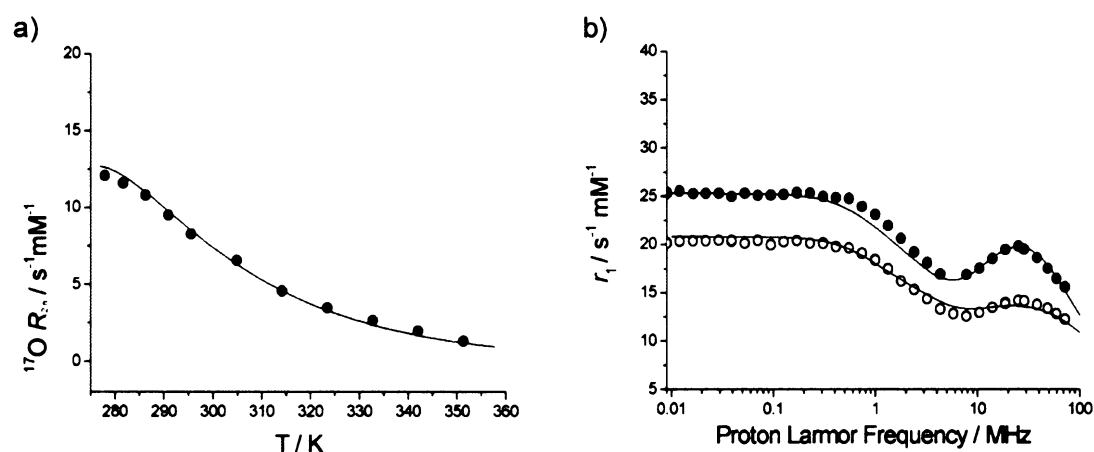

Figure 3.13. The relaxometric characteristics for G2-(DO3A-P^{NBn})$_{16}$ conjugate: a) ^{17}O transversal, R_2, relaxation rates at 12.2 MHz and pH 7; b) ^{1}H NMRD profiles at 25 (full circles) and 37 °C (open circles) at pH = 7.

characteristic for the contemporary conjugated CAs candidates and the internal flexibility needs to be controlled to move ahead.

The approach I have taken in order to address the internal flexibility relies on an interaction between the negatively charged conjugates (each chelate unit contributes by one negative charge) and positively charged polyaminoacids. In particular, the poly(arginines) and poly(lysines) of a variable chain length were used. The experimental setup was to titrate solution of the conjugate at a fixed concentration with an increasing amount of the polyaminoacid.

For all systems, a relaxivity step on a titration curve was detected at the point where the theoretical balance of positive/negative charges was reached (Figure 3.14a).

Moreover, in several conjugate/polyaminoacid systems, a precipitation occurred in the same area but it dissolved again by a further addition of polyaminoacid. To prove an electrostatic basis of this effect, I performed a blank titration with a polyglutamic acid where no enhancement of relaxivity was observed (Figure 3.14b). The quantitative analyses of the relaxivity enhancement factors resulted in two general outcomes:
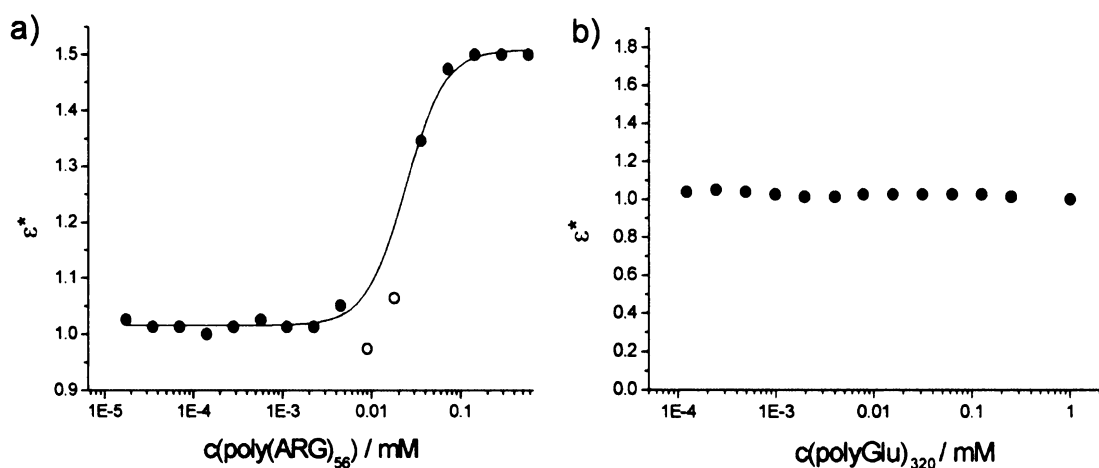
Figure 3.14. The plots of relaxivity-enhancement factor as a function of polyaminoacid concentration (in logarithmic scale) for the $G2$-$(Gd$-$DO3A$-$P^{NBn})_{16}$ conjugate with (a) poly(arginine)$_{56}$ and (b) poly(glutamic acid)$_{320}$. The solid line is the sigmoidal fit just to guide the eyes. The experimental points represented by the open circles mark the solutions where a precipitation occurred. Both titrations were done at 20MHz and 25 °C.

(i)   at a given length of polyaminoacid, the relaxivity enhancement decreases with an increasing size of the conjugate molecule.

(ii)   at a fixed size of the conjugate, the relaxivity increases by increasing a chain length of the polyaminoacid up to the certain point and then no further.

These observations were reasoned by considering the size proportions of an adduct components (Figure 3.15). As a thread of the polyaminoacid of a fixed chain length interacts with a conjugate molecule, it may wrap a small conjugates around whereas the bigger ones are just "touched". Also, in adducts with higher-molecular conjugates, the global reorientation is fractionally less affected than in the other cases. In consequence, the maximal relaxivity enhance-
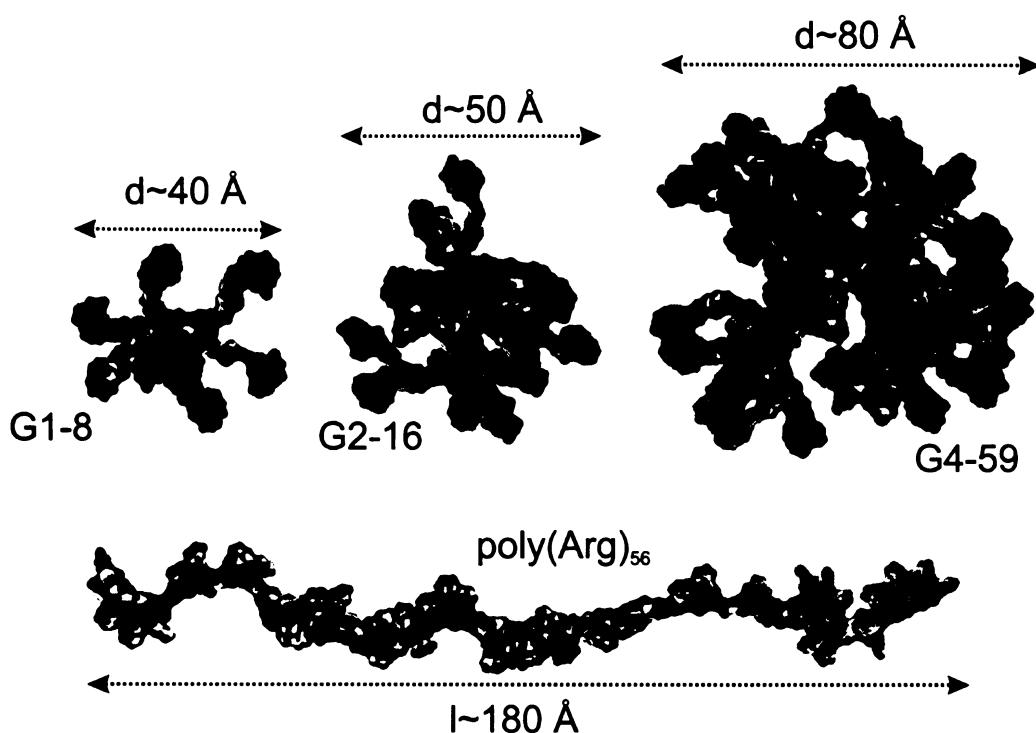
Figure 3.15. The illustration of the size proportions of adducts components. The drawings are based on snapshots from a molecular modeling.

ment factor, ε^b, dropped from 1.8 for the G1-(Gd-DO3A-P^{NBn})$_8$ conjugate to 1.4 for the G4-(Gd-DO3A-P^{NBn})$_{59}$ conjugate in the presence poly(Arg)$_{320}$. On the other hand, for the particular conjugate molecule, further increase of a polyaminoacid chain leads only to a formation of a multimer where the independent interacting sites can move freely and the relaxivity enhancement is not coupled with the increase of the overall molecular weight. To witness the quantitative effect of the adduct formation, I have measured the ^{1}H NMRD profiles and the relaxivity as a function of temperature for G2-(DO3A-P^{NBn})$_{16}$-poly(Arg)$_{56}$ adduct; the data were then analyzed using the Lipari-Szabo approach (Table 3.3).[107] It was confirmed that the relaxivity enhancement can be ascribed not only to a diminution of a global tumbling rate but, even to a larger extent, to a partial "freezing" of the internal motion. Consequently, the molecules of polyaminoacids behave like a "molecular glue" sticking different part of a conjugate surface and/or conjugate molecules together.

Finally, the adduct formation in response to a pH value was explored. Interestingly, I found that in G2-(Gd-DO3A-P^{NBn})$_{16}$-poly(Lys)$_{61}$ system, the resulting relaxivity is a steep function of pH in the region of pK_a of the lysine residues. The explanation is quite straightforward: as the aminoacid chain become deprotonated, the adduct breaks apart. In opposite, the G2-(Gd-DO3A-P^{NBn})$_{16}$-poly(Arg)$_{54}$ adduct proved to be insensitive to pH (in range 2–12) owning to a rather high pK_a values of the arginine moieties. The whole concept of pH-responsive non-covalent adducts formation as a way to increase a relaxivity may be used in chemically responsive CAs or in molecular imaging.

47

4. Conclusions

$\mathcal{I}$n my PhD Thesis, I studied several potential contrast-enhancing systems for MRI tomography conceptually based on a macrocyclic ligands bearing one phosphorus-containing pendant arm. The project was divided into four main parts. The first part dealt with a study of lanthanide(III) complexes of the simple monophosphonate DOTA analogue, DO3AP, in a view to explore an influence of the phosphorus acid moiety on complex structure and dynamics. Then, in the next step, the ligand structure was modified to benzylmonophosphinate leading to DO3A-P^{NBn} and DO3A-P^{ABn} structures in order to introduce a bifunctionality. In order to proceed toward more sophisticated agents, the ditopic ligand, CS(DO3A-$P^{Bn(N)}$)$_2$, was subsequently synthesized. In the final step, the bifunctional monophosphinate DOTA analogue was attached to the PAMAM dendrimeric carriers to take an advantage from a covalent conjugation. All systems were studied predominantly in solution with multinuclear NMR and relaxometric techniques.

The in-depth study based on ^{31}P and ^{1}H NMR on the DO3AP lanthanide(III) complexes showed that the presence of a phosphorus acid moiety induces a significantly higher abundance of the desired TSAP isomer. In particular, in the Eu(III) complex, the TSAP/SAP ratio was about 1:1 in contrast to the Eu-DOTA complex where the ratio 0.2:0.8 was found. Moreover, at the end of the lanthanide series, a much higher population of a "dehydrated" TSAP' isomer is supposed in comparison to Ln-DOTA. The relevant relaxometric characteristics were assessed on the Gd-DO3AP complex. The most crucial parameter, the water residence lifetime $^{298}\tau_M$, was found to be 14 ns at pH 7. This was ascribed to a bulkiness of the phosphonate acid pendant promoting a water exchange by steric compressions around the water-binding site. Ln(III) complexes of DO3AP were also characterized at variable pH in order to investigate an effect of protonation on complex properties like a speciation in solution and/or water exchange rate. It was proved that with the protonation, the abundance of TSAP for heavy lanthanides grows up and a water residence lifetime, $^{298}\tau_M$, determined for the Gd(III) complex increases from 14 ns at pH 7 to 40 ns at pH 4.7. This was not fully ambiguously accounted either for an influence of the second-sphere or for an electrostatic effects.

The solution behavior of the Ln(III) complexes of both monophosphinates DO3A-P^{ABn} and DO3A-P^{NBn} partly parallels that of DO3AP. The abundance of TSAP isomer along the lanthanide series was quite similar for complexes of all three phosphorus-containing ligands. On the

contrary, both phosphinates proved to be unaffected by change of pH in range 2–12, as was expected. Interestingly, comparing the relaxometric characteristics of their Gd(III) complexes, they showed rather different water residence lifetimes $^{298}\tau_M$ (16 and 52 ns, respectively) and also rotational correlation times $^{298}\tau_R$ (88 and 163 ps, respectively). The observed differences were explained by a different arrangement of the benzyl moiety in both systems. Finally, as the Gd(III) complexes of these simple ligands exhibit somewhat higher values of relaxivity, it is likely they benefit from a contribution of the second hydration sphere. To take an advantage of the fast water exchange in covalent high molecular weight conjugates, the aminobenzyl derivative DO3A-P^{ABn} was modified to a highly reactive isothiocyanate. The first conjugate prepared was a ditopic analogue of DO3A-P^{ABn} joined by a thiourea linker - CS(DO3A-P$^{Bn(N)}$)$_2$. The corresponding bis-Gd(III) complex, though originally designed only as a model compound, proved to be a quite promising CA candidate for its low water residence lifetime ($^{298}\tau_M$ = 53 ns) and a quite compact structure exhibiting a relatively slow molecular tumbling rate ($^{298}\tau_R \sim$ 190 ps). Its relaxivity (r_1 = 6.2 s^{-1}mM^{-1} at 37 °C and 20 MHz) seems to be one of the highest among mono-hydrated (q = 1) dimeric systems studied so far.

The last objective was a conjugation of the monophosphinate ligand to PAMAM dendrimers of various sizes, namely generation 1, 2 and 4. The relaxivity of the corresponding gadolinium(III) complexes were initially characterized by variable pH study to exploit the well-known pH-responsive structural behavior of the PAMAM structures. It was found that under acidic condition, the relaxivity could be up to 30% higher than in alkaline solution owning to a more rigid and more expanded structure of the conjugate. The relaxometric data were processed by means of the Lipari-Szabo approach. Despite a favorable water residence lifetime (~50–70 ns), relaxivities were only moderate due to a high flexibility of the structure. To partly control the internal motion, the cationic polyaminoacids like poly(lysines) or poly(arginines) were successfully tested. It was demonstrated that a sufficiently long thread of a polyaminoacid may act like a "molecular glue" forming an electrostatic supramolecular adducts with a conjugate molecule. Using this concept, it was possible to attain up to 80% increase in relaxivity. Additionally, as the overall charge on a polyaminoacid (e.g. poly(lysine)) chain depends on pH value, the adduct formation and, in turn, the relaxivity could be effectively pH-controlled.

To conclude, in my Thesis I found that ligands with phosphorus acid pedant arm substituting carboxylate in DOTA structure are endowed with several favorable features like a water residence lifetime optimal for a preparation of high-relaxivity covalent conjugates. Importantly, these promising properties were proved to persist even after the conjugation as was demonstrated on a symmetrical ditopic model compound for the first time. Importantly, the following study of low-generation PAMAM conjugate proved that, unlike most of the published studies, the relaxivity of these macromolecular systems is not exchange-limited. This has allowed me to

investigate in detail the limiting effects on the relaxivity of the internal rotation of the complex in the conjugates. In addition, I shown that the local motions of the dendrimer backbone and of the conjugated complexes can be slowed down by a formation of supramolecular adducts with cationic polyaminoacids. Also, I was able to quantitatively evaluate the effects of the local motions and to effectively reduce them. As a result, the efficacy of these systems as relaxation agents is the highest so far reported for this class of compounds that can find a variety of potential biomedical/bioinorganic applications.

For the close future, we plan *in vivo* tests of these conjugated Gd(III) complexes on mice to explore their pharmacokinetics, stability and distribution in organism. In ligand design, the negative impact of the internal mobility needs to be urgently addressed. The research currently under way in our group, is focused on a preparation of a fast-exchanging Gd(III) chelate able to be covalently conjugated to a macromolecular carrier in a ditopic fashion. That should, in theory, avoid the internal mobility substantially and, in turn, allow achieving really high relaxivities.

5. References

[1] The official web-site of the Nobel committee, http://nobelprize.org/, **2006.**

[2] R. Damadian, Science, **1971,***171*,1151.

[3] *"A Machine Called Indomitable"*, by New York Times reporter Sonny Kleinfield, *Times Books, Inc.*, **1985**.

[4] R.V. Damadian, US Pat. 3,789,832, **1974**.

[5] P.C. Lauterbur, "Image formation by induced local interactions: examples employing nuclear magnetic resonance.", *Nature* **1973**, *242*,190.

[6] P. Mansfield and P.K. Grannell, „NMR 'diffraction' in solids?", *J Phys C: Solid State Phys.* **1973**, *6*, 422.

[7] P.C. Lauterbur, " Magnetic resonance zeugmatography", *Pure Appl. Chem.* **1974**, *40*, 149.

[8] P. Mansfield and P.K. Grannell, ""Diffraction" and microscopy in solids and liquids by NMR", *Phys. Rev. B* **1975**, *12*, 422.

[9] A. Kumar, D. Welti and R. Ernst, "NMR Fourier zeugmatography.", *J. Magn. Res.* **1975**, *18*, 69.

[10] Adopted from the official website of MRI FBMI ČVUT laboratories, Prague, http://www.fbmi.cvut.cz/mri/, **2006.**

[11] *"The Chemistry of Contrast Agents in Medical Magnetic Resonance Imaging"*, A. E. Merbach and É. Tóth (Eds.), John Wiley & Sons, Chichester (England), **2001.**

[12] a) J. Belliveau, B. Rosen, H. Kantor, R. Rzedzian, D. Kennedy, R. McKinstry, J. Vevea, M Cohen, I. Pykett and T. Brady, *Magn. Reson. Med..* **1990**, *14*, 538; b) S. Ogawa, T.-M. Lee, A. S. Nayak and P. Glynn, *Magn. Reson. Med.* **1990**, *14*, 68.

[13] V. M. Runge, M. A. Foster, J. A. Clanton, M. M. Jones, C. M. Lukehart, J. M. Hutchison, J. R. Mallard, F. W. Smith, C. L. Partain and A. E. James Jr, *Radiology* **1984**, *152*, 123.

[14] N. Krasnow, *Biochem.Biophys. Acta* **1972**, *282*, 187.

[15] H. Friebolin, *"Basic One- and Two-Dimensional NMR spectroscopy"*, VCH (Germany), **2005.**

[16] a) T. Shen, R. Weissleder, M Papisov, A. Bogdanov and T. Brady, Magn. Reson. Med. **1993**, *29*, 599. b) R.N. Muller *"Encyclopedia of Nuclear Magnetic Resonance"*, D. M.Grant and R.K. Harris (Eds.), John Wiley & Sons, Chichester (England), **1995**, p 1438–1344.

[17] *"Magnetic Resonance Imaging. Theory and Practice"*, M. T. Vlaardingerbroek and J. A. den Boer, Springer Verlag (Germany), **1996.**

[18] W. P. Cacheris, S. C Quay and S. M. Rocklage, *Magn. Reson. Imag.* **1990**, *8*, 467.

[19] K. Kumar, C. A. Chang, L. C. Francesconi, D.D Dischino, M.F.Malley, J. Z. Gougoutas and M. F. Tweedle, *Inorg. Chem.* **1994**, *33*, 3567.

[20] MRI web information portal; http://www.mr-tip.com/serv1.php, **2006**.

[21] R. M. Smith, R. J. Motekaitis and A. E. Martell, *NIST StandardReference Database No.46*, (3.0 ed.), National Institute of Standards and Technology, Washington, DC, **1997**.

[22] É. Tóth, R. Király, J. Platzek, B. Radüchel, E. Brüche, *Inorg. Chim. Acta* **1996**, *249*, 191.

[23] D. J.Parmelee, R. C. Walovitch, H. S. Ouellet and R. B. Lauffer. *Invest. Radiol.* **1997**, 32(12), 741.

[24] P. Caravan, C. Comuzzi, W. Crooks, TJ McMurry, GR Choppin, SR Woulfe, Inorg. Chem. **2001**, 40(9), 2170.

[25] D. A. White, L. A. de Learie, D. A. Moore, R. A. Wallace, T. J. Dunn, W. P. Cacheris, H. Imura and G .R. Choppin, *Invest. Radiol.* **1991**, *26*, 5226.

[26] F. Uggeri, S. Aime, P. L. Anelli, M. Botta, M. Brocchetta, C. de Haën, G. Ermondi, M. Grandi and P. Paoli, *Inorg. Chem.* **1995**, *34*, 633.

[27] P. Caravan, J. J. Ellison, T. J. McMurry and R. B. Lauffer, *Chem. Rev.* **1999**, *99,* 2293.

[28] J. A. Peters, J. Huskens and D. J. Raber, *Prog. NMR Spectrosc.* **1996**, *32*, 283.

[29] M. Botta, *Eur. J. Inorg. Chem.*, **2000**, 399.

[30] a) S. Aime, A. S. Batsanov, M. Botta, R. S. Dickins, S. Falkner, C. E.Foster, A. Harrison, J. A. K. Howard, J. M. Moloney, T. J. Norman, D. Parker and J. A. G. Williams, *J. Chem. Soc. Dalton Trans.* **1997**, 3623; b) S. Aime, A. S. Batsanov, M. Botta, J. A. K. Howard, D. Parker, K. Senanayake and J. A. G. Williams, *Inorg. Chem.* **1994**, *33*, 4696.

[31] S. Zhang, K. Wu and A. D. Sherry, *Angew. Chem.*, **1999**, *111*, 3382.; *Angew. Chem. Int. Ed.* **1999**, *38*, 3192.

[32] P. Caravan, M. T. Greenfield, X. Li and A. D. Sherry, *Inorg. Chem.* **2001**, *40*, 6580.

[33] a) the official Bruker Biospin website: http://www.bruker-biospin.com/; b) the official Siemens web-site: http://www.medical.siemens.com; c) the official Varian website: http://www.varianinc.com/.

[34] a) S. Rast, A. Borel, L. Helm, E. Belorizky, P. H. Fries and A. E. Merbach, *J. Am. Chem. Soc.* **2001**, *123*, 2637; b) S. Rast, P. H. Fries, P. H. Belorizky, A. Borel, L. Helm and A. E. Merbach, *J. Chem. Phys.* **2001**, *115*, 7554; c) F. A. Dunand, A. Borel and L. Helm, *Inorg. Chem. Commun.* **2002**, *5*, 811.

[35] X. Zhou, P. Caravan, R. B. Clarkson and P.-O. Westlunda, *J. Magn. Reson.* **2002**, *167*, 147.

[36] D. H. Powell, O. M. N. Dhubhghaill, D. Pubanz, L. Helm, Y. S. Lebedev, W. Schlaepfer and A. E. Merbach, *J. Am. Chem. Soc.* **1996**, *118*, 9333.

[37] M. Woods, M. Botta, S. Avedano, J. Wang and D. A. Sherry, *Dalton Trans.*, **2005**, 3829.

[38] S. Aime, M. Botta, S. G. Crich, G. Giovenzana, R. Pagliarin, M. Piccinini, M. Sisti and E. Terreno, *Magn. Reson. Chem.*, **1998**, *36*, S200.

[39] S. Hajela, M. Botta, S. Giraudo, J. Xu, K. N. Raymond and S. Aime, *J. Am. Chem. Soc.* **2000**, *122,* 11228.

52

[40] R. Ruloff, É. Tóth, R. Scopelliti, R. Tripier, H. Handel and A. E. Merbach, *Chem. Commun.*, **2002**, 2630.

[41] M. Polášek, J. Rudovský, P. Hermann, I. Lukeš, L. V. Elst and R. N. Muller, *Chem. Commun.* **2004**, 2602.

[42] a) D. Pubanz, G. Gonzalez, D. H. Powell, A. E. Merbach, *Inorg. Chem.* **1995**, *34*, 4447; b) N. Graeppi, D. H. Powell, G. Laurenczy, L. Zekany, A. E. Merbach, *Inorg. Chim. Acta* **1995**, *235*, 311.

[43] M. Woods, Z. Kovacs, S. Zhang and A. D. Sherry, *Angew. Chem., Int. Ed.* **2003**, *42*, 5889.

[44] D. A. Fulton, M. O'Halloran, D. Parker, K. Senanayake, M. Botta and S. Aime, *Chem. Commun.*, **2005**, 474.

[45] D. A. Fulton, E. M. Elemento, S. Aime, L. Chaabane, M. Botta and David Parker, *Chem. Commun.* **2006**, 1064.

[46] J. P. André, É. Tóth, H. Fischer, A. Seelig, H. R. Mäcke and A. E. Merbach, *Chem. Eur. J.* **1999**, *5*, 2977.

[47] L. Lattuada and G. Lux, *Tetrahedron Lett.* **2003**, *44*, 3893.

[48] G. M. Nicolle, E. Tóth, K.-P. Eisenwiener, H. R. Mäecke, A. E. Merbach, *J. Biol. Inorg. Chem.*, **2002**, *7*, 757.

[49]) a) T. N. Parac-Vogt, K. Kimpe, S. Laurent, C. Piérart, L. Vander Elst, R. N. Muller and K. Binnemans, *Eur. J. Inorg. Chem.* **2004**, 3538; b) T.N. Parac-Vogt, K. Kimpe, S. Laurent, C. Pierart, L. Vander Elst, R. N. Muller and K. Binnemans, *Eur. Biophys. J.* **2006**, *35*, 136.

[50] R. B. Lauffer, D. Parmelee, S. U. Dunham, H. S. Ouellet, R. P. Dolan, S. Witte, T. McMurry and R. C. Walovitch, *Radiology*, **1998**, *207*, 530.

[51] G. M. Nicolle, E. Tóth, H. Schmitt-Willich, B. Radüchel and A. E. Merbach, *Chem. Eur. J.* **2002**, *8*, 1040.

[52] É. Tóth, D. Pubanz, S. Vauthey, L. Helm and A. E. Merbach, *Chem. Eur. J.* **1996**, *2*, 1607.

[53] S. Laus, A. Sour, R. Ruloff, E. Tóth, A. E. Merbach, *Chem. Eur. J.* **2005**, *11*, 3064.

[54] S. Aime, M. Botta, M. Fasano, M. P. M. Marques, C. F. G. C. Geraldes, D. Pubanz and A. E. Merbach, *Inorg. Chem.* **1997**, *36*, 2059.

[55] S. Aime, L. Barbero, M. Botta and G. Ermondi, *Inorg. Chem.* **1992**, *31*, 4291.

[56] P. Vojtíšek, P. Cígler, J. Kotek, J. Rudovský, P. Hermann and Ivan Lukeš, *Inorg. Chem.* **2005**, *44*, 5591.

[57] M. R. Spirlet, J. Rebizant, J. F. Desreux, M. F.Loncin, *Inorg. Chem.* **1984**, *23*, 359.

[58] C. A. Chang, L. C. Francesconi, M. F. Malley, K. Kumar, J. Z. Gougoutas, M. F. Tweedle, D. W. Lee and L. J. Wilson, *Inorg. Chem.*, **1993**, *32*, 3501.

[59] S. Aime, A. Barge, M. Botta, M. Fasano, J. D. Ayala and G. Bombieri, *Inorg. Chim. Acta* **1996**, *246*, 423.

[60] S. Aime, A. Barge, F. Benetollo, G. Bombieri, M. Botta and F. Uggeri, *Inorg. Chem.* **1997**, *36*, 4287.

[61] David Parker, *Chem. Soc. Rev.* **2004**, *33*, 156.

[62] a) S. Zhang, Z. Kovacs, S. Burgess, S. Aime, E. Terreno and A. D. Sherry, *Chem. Eur. J.* **2001**, *7*, 288; b) M. Woods, S. Aime, M. Botta, J. A. K. Howard, J. M. Moloney, M. Navet, D. Parker, M. Port and O. Rousseaux, *Am. Chem. Soc.* **2000**, *122*, 9781; c) F. A. Dunand, R. S. Dickins, D. Parker and A. E. Merbach, *Chem.Eur. J.* **2001**, *7*, 5160.

[63] S. Aime, A. S. Batsanov, M. Botta, J. A. K. Howard, D. Parker, K. Senanayake, G. Williams, *Inorg. Chem.* **1994**, *33*, 4696; b) S. Aime, A. S. Batsanov, M. Botta, R. S. Dickins, S. Faulkner, C. E. Foster, A. Harrison, J. A. K. Howard, J. M. Moloney, T. J. Norman, D. Parker, L. Royle and J. A. Gareth Williams, *J. Chem. Soc., Dalton Trans.* **1997**, *3623*.

[64] S. Aime, A. S. Batsanov, M. Botta, R. S. Dickins, S. Faulkner, C. E. Foster, A. Harrison, J. A. K. Howard, J. M. Moloney, T. J. Norman, D. Parker, L. Royle and J. A. G. Williams, *J. Chem.Soc., Dalton Trans.* **1997**, 3623.

[65] K. P. Pulukkody, T. J. Norman, D. Parker, L. Royle and C. J. Broan, *J. Chem. Soc., Perkin Trans. 2* **1993**, 605.

[66] W. D. Kim, G. E. Kiefer, J. Huskens and A. D. Sherry, *Inorg. Chem.* **1997**, *36*, 4128.

[67] J. Rohovec, P. Vojtíšek, P. Hermann, J. Mosinger, Z. Žák and I. Lukeš, *J. Chem. Soc., Dalton Trans.*, **1999**, 3585.

[68] R. C. Brasch, *Magn. Reson. Med.* **1991**, *22*, 282.

[69] R. B. Lauffer and T. J. Brady, *Magn. Reson. Imag.* **1985**, *17*, 202.

[70] S. Aime, M. Botta, S. Geninatti-Crich, G. Giovenzana, G. Palmisano and M. Sisti, *Bioconjugate Chem.* **1999**, *10*, 192.

[71] M. Spanoghe, D. Lanens, R. Dommisse, A. Van der Linden and F. Alderweireldt, *Magn. Res. Imag.* **1992**, *10*, 913.

[72] P. Niemi, T. Riesto, I. Hemmilä and M. Kormano, *Invest. Radiol.* **1991**, *26*, 820.

[73] A. D. Sherry, W. P. Cacheris and K.-T. Kuan, *Magn. Reson. Med.* **1988**, *8*, 180.

[74] T. Desser, D. Rubin, H. Muller, F. Qing, S. Khodor, S. Zanazzi Young, D. Ladd, J. Wellons, K. Kellar, J. Toner, and R. Snow, *J. Magn. Reson. Imag.* **1994**, *4*, 467.

[75] E. C. Wiener, M. W. Brechbiel, H. Brothers, R. L. Magin, O. A. Gansow, D. A. Tomalia and P. C. Lauterbur, *Magn. Reson. Med.* **1994**, *31*, 1.

[76] R. Esfand and D. A. Tomalia, *Drug. Discov. Today*, **2001**, *6*, 427.

[77] P. F. Sieving, A. D. Watson, S. M. Rocklage, *Bioconjugate Chem.* **1990**, *1*, 65.

[78] R. Rebizak, M. Schaefer and E. Dellacherie, *Bioconjugate Chem.* **1998**, *9*, 94.

[79] a) C. Wu, M. W. Brechbiel, R. W. Kozak and O. A. Gansow, *Bioorg. Med. Chem. Lett.* **1994**, *4*, 449; b) E. C. Wiener, S. Konda, A. Shadron, M. Brechbiel, O. Gansow, *Invest. Radiol.* **1997**, *32*, 748.

[80] S. Aime, M. Botta, L. Frullano, S. Geninatti-Crich, G. B. Giovenzana, R. Pagliarin, G. Palmisano and M. Sisti, *Chem. Eur. J.* **1999**, *5*, 1253.

[81] J. Rudovský, P. Cígler, J. Kotek, P. Hermann, P. Vojtíšek, I. Lukeš, J. A. Peters, L. Vander Elst and R. N. Muller, *Chem. Eur. J.* **2005**, *11*, 237.

[82] a) P. Lebdušková, P. Hermann, L. Helm, É. Tóth, J. Kotek, K. Binnemans, J. Rudovský, I. Lukeš and A. E. Merbach, *in preparation*; b) Petra Lebduskova, PhD Thesis (in English), Charles University in Prague, **2006**.

[83] Petr Cígler, Ms. Thesis (in Czech), Charles University in Prague, **2001**.

[84] D. H. Powell, O. M. N. Dhubhghaill, D. Pubanz, L. Helm, Y. S. Lebedev, W. Schlaepfer and A. E. Merbach, *J. Am. Chem. Soc.* **1996**, *118*, 9333.

[85] J. P. André, H. R. Maecke, É. Tóth and A. E. Merbach, *J. Biol. Inorg. Chem.* **1999**, *4*, 341.

[86] E. Szilágyi, É. Tóth, E. Brücher and A. E. Merbach, *J. Chem. Soc. Dalton Trans.* **1999**, 2481.

[87] Z. Jandurová, J. Kotek , J. Rudovský, P. Hermann , R. N. Muller, J. A. Peters and Ivan Lukeš, **2006**, *unpublished results.*

[88] M. Šedinová, *2005*, Bc.Thesis (in Czech), Charles University, **2005**.

[89] J. Rudovský, J. Kotek, P. Hermann, I. Lukeš, V. Mainero and S. Aime, *Org. Biomol. Chem.* **2005**, *3*, 112.

[90] J. Kotek, J. Rudovský, P. Hermann and Ivan Lukeš, *Inorg. Chem.* **2006**, *45*, 3097.

[91] E. Terreno, P. Boniforte, M. Botta, F. Fedeli, L. Milone, S. Mortillaro and S. Aime, *Eur. J. Inorg. Chem.* **2003**, *19*, 3530.

[92] J. Rudovský, Ms.Thesis (in Czech), Charles University in Prague, **2002**

[93] D. H. Powell, O. M. N. Dhubhghaill, D. Pubanz, L. Helm, Y. S. Lebedev, W. Schlaepfer and A. E. Merbach, *J. Am. Chem. Soc.* **1996**, *118*, 9333.

[94] É. Tóth, S. Vauthey, D. Pubanz and A. E. Merbach, *Inorg. Chem.* **1996**, *35*, 3375.

[95] E. Zitha-Bovens, L. Vander Elst, R. N. Muller, H. van Bekkum and J. A. Peters, *Eur. J. Inorg. Chem.* **2001**, 3101.

[96] T.-M. Lee, T.-H. Cheng, M.-H. Ou, C. A. Chang, G.-C. Liu and Y.-M. Wang, *Magn. Reson. Chem.* **2004**, *42*, 329.

[97] a) W. H. Li, S. E. Fraser and T. J. Meade, *J. Am. Chem. Soc.* **1999**, *121*, 1413; b) W. H. Li, G. Parigi, M. Fragai, C. Luchinat and T. J. Meade, *Inorg. Chem.* **2002**, *41*, 1418.

[98] a) R. Ruloff, G. van Koten and A. E. Merbach, *Chem. Commun.* **2004**, 842; b) J. B. Livramento, É. Tóth, A. Sour, A. Borel, A. E. Merbach and R. Ruloff, *Angew. Chem. Int. Ed.* **2005**, *44*, 1480; c) J. Costa, R. Ruloff, L. Burai, L. Helm and A. E. Merbach, *J. Am.Chem. Soc.* **2005**, *127*, 5147; d) J. Costa, É. Tóth, L. Helm and A. E. Merbach, *Inorg. Chem.* **2005**, *44*, 4747.

[99] J. Rudovský, M. Botta, P. Hermann, A. Koridze and S. Aime, *Dalton Trans.* **2006,** DOI: 10.1039/b518147j.

[100] P. K. Maiti, T. Çagin, G. Wang, W. A. Goddard III, *Macromolecules,* **2004,** *37,* 6236.

[101] a) E. C. Wiener, M. W. Brechbiel, H. Brothers, R. L. Magin; A. Gansow, D. A. Tomalia and P. C. Lauterbur, *Magn. Reson. Med.* **1994**, *31*, 1; b) V. J. Venditto, C. A. S. Regino and M. W. Brechbiel, *Mol. Pharmaceutics* **2005**, *2*, 302; c) H. Kobayashi and M. W. Brechbiel, *Curr. Pharm. Biotechnol.* **2004**, *5*, 539.

[102] L. D. Margerum, B. K. Campion, M. Koo, N. Shargill, J.-J. Lai, A. Marumoto, and P. C. Sontum, *J. Alloys Compd,.* **1997**, *249*, 185.

[103] S. Laus, A. Sour, R. Ruloff, É. Tóth, A. E. Merbach, *Chem. Eur. J.* **2005**, *11*, 3064.

[104] W. Chen, D. A. Tomalia and J. L. Thomas, *Macromolecules* **2000**, *33,* 9169.

[105] J. Rudovský, P. Hermann, M. Botta, S. Aime, I. Lukeš, *Chem. Commun.* **2005**, 2390.

[106] J. Rudovský, M. Botta, P. Hermann, K. I. Hardcastle, I. Lukeš and Silvio Aime, submitted to *J. Am. Chem. Soc.* **2006**.

[107] a) G. Lipari and S. Szabo, *J. Am. Chem. Soc.* **1982**, *104*, 4546; b) G. Lipari and S. Szabo, *J. Am. Chem. Soc.* **1982**, *104*, 4559.

[108] S. Aime, M. Botta, M. Fasano, S. Geninatti Crich and E. Terreno, *J. Biol. Inorg. Chem.* **1996**, *1*, 319

Appendix 1 – Theory of lanthanide-induced magnetic relaxation

Generally, paramagnetic lanthanide ions are able to enhance both, the longitudinal, R_1 $(=1/T_1)$, and the transversal, R_2 $(=1/T_2)$, relaxation rates of nuclei which get to a vicinity of a metal ion. As the mechanism on which the effect of Gd-based MRI CAs inheres in a magnetic interaction of tissue water with a Gd(III) metal centre of agent, the following text is particularly focused on interaction between Gd^{3+} ion and nuclei of ^{17}O and ^1H of surrounding water molecules. In dependence of a structure and coordination number of gadolinium, the water molecules may diffuse to an outer-, second- or inner-hydration spheres of a paramagnetic complex and they may exchange the magnetic information though space or *via* direct bond interaction with the Gd^{3+} ion.

^{17}O NMR spectroscopy

In systems, where water molecules are directly coordinated to Gd(III) metal center, the inner-sphere contribution was shown to be the major factor affecting T_1 or T_2 relaxation rates of ^{17}O, whereas the later two contributions (second-sphere and outer-sphere) could be neglected.[1] Of course, only a minor fraction of water molecules are instantly bound to Gd(III) as the molar concentration of water is about 55.56 M whereas the one of CA is typically in range 1-100 mM in analytical samples. Consequently, in a fast-exchange regime (an exchange of water is much faster than a timescale of an NMR measurement) the observed values are weighted averages between a bulk- and bound-water ^{17}O relaxation rates. Numerically, these are given by Connick-Swift equations (1) and (2)[2]

$$\frac{1}{T_{1,obs}} = \frac{qc_{Gd}}{T_{1,M} + \tau_m} + \frac{1}{T_{1,dia}} \tag{1}$$

$$\frac{1}{T_{2,obs}} = \frac{qc_{Gd}}{\tau_M}\left[\frac{T_{2,M}^{-2} + \tau_M^{-1} + \Delta\omega_M^{\,2}}{\left(\tau_M^{-1} + T_{2,M}^{-1}\right)^2 + \Delta\omega_M^{\,2}}\right] + \frac{1}{T_{2,OS}} + \frac{1}{T_{2,dia}} \tag{2}$$

where q is a number of water molecules in the first coordination sphere of the complex, c_{Gd} is the concentration of Gd(III) ion, τ_M is the water residence lifetime, $T_{i,M}$ are the pure relaxation times of ^{17}O in bound water molecules, $T_{2,OS}$ is the second-sphere contribution to overall R_2 relaxation rate and $T_{i,dia}$ are the diamagnetic contributions. Practically, T_1 relaxation rates of ^{17}O

are usually measured by an inversion-recovery experiment[3] and T_2 by the Carr-Purcell-Meiboom-Gill pulse sequence.[4] The observed rates are then corrected for the diamagnetic contribution by measuring a diamagnetic complex (La(III), Lu(III), Y(III)) of the ligand under study. The relaxation times of ^{17}O nuclei directly bound to Gd(III) can be, in general, further separated into several contribution as shown in equation (3),

$$\frac{1}{T_{i,M}} = \frac{1}{T_{i,c}} + \frac{1}{T_{i,p}} + \frac{1}{T_{i,\chi}} + \frac{1}{T_{i,q}} \qquad \text{for } i = 1,2 \tag{3}$$

where T_c represents through-bound (or contact) contribution, T_p through-space (pseudocontact or dipolar) contribution, T_χ is Curie contribution and T_q the quadrupolar contribution.[5] Strictly speaking, the last two relaxation mechanisms also stems from the through-space interaction between Gd(III) and ^{17}O nucleus.

Focusing on longitudinal $T_{1,M}$ relaxation time, the most influential are the "$T_{1,p}$" and "$T_{1,q}$" terms given by Solomon-Bloembergen equation (4)[6] and equation (5)[5]:

$$\frac{1}{T_{1,d}} = \frac{2}{15}\left(\frac{\mu_0}{4\pi}\right)^2 \frac{\gamma_I^2 \mu_{eff}^2 \beta^2}{r_{GdO}^6} \left[\frac{3\tau_{1,d}}{1 + \omega_I^2 \tau_{1,d}^2} + \frac{7\tau_{2,d}}{1 + \omega_S^2 \tau_{2,d}^2}\right] \tag{4}$$

$$\frac{1}{T_{1,q}} = \frac{3\pi^2}{10}\left(\frac{\mu_0}{4\pi}\right)^2 \frac{2I+3}{I^2(2I-1)} \chi^2\left(1 + \frac{\eta^2}{3}\right)\tau_R \tag{5}$$

There γ_I is the nuclear gyromagnetic ratio of ^{17}O nucleus ($\gamma_I = -3.626 \times 10^7$), μ_{eff} is the effective magnetic moment of Gd^{3+} ion (μ_{eff}(Gd)=7.94 B.M.), β is the Bohr magneton (9.274×10^{-24} A m^2), r_{GdO} is the length of bound vector between Gd(III) ion and oxygen of coordinated water (typically fixed to 2.5–2.6 Å based on X-ray structures), ω_I and ω_S are ^{17}O nuclear and electronic angular frequencies, respectively, μ_0 is the susceptibility of vacuum ($4\pi \times 10^{-7}$), I is the spin quantum number for ^{17}O nucleus ($I = 5/2$), χ is the quadrupolar coupling constant, η is an asymmetry parameter and $\tau_{i,d}$ are the total dipolar correlation times given by equation (6)[7]:

$$\frac{1}{\tau_{i,d}} = \frac{1}{\tau_M} + \frac{1}{\tau_R} + \frac{1}{T_{i,e}} \qquad \text{for } i = 1,2 \tag{6}$$

where $T_{i,e}$ are the electronic relaxation times. It was shown that the $T_{1,e}$ and $T_{2,e}$ electronic spin relaxation times for ions with $I > 1/2$ are governed mainly by a transient zero-field splitting (ZFS)[5] and a spin-rotation (SR) mechanism of relaxation (Equation (7))[8]:

$$\frac{1}{T_{i,e}} = \left(\frac{1}{T_{i,e}}\right)^{ZFS} + \left(\frac{1}{T_{i,e}}\right)^{SR} \qquad \text{for } i = 1,2 \tag{7}$$

As long as a complex can be approximated by a regular octahedron reorienting isotropically in solution, ZFS contribution are well described by the Bloembergen-Morgan equations (8) and (9).[7]

$$\left(\frac{1}{T_{1,e}}\right)^{ZFS} = \frac{1}{25}\Delta^2\tau_V\left[4S(S-1)-3\right]\left(\frac{1}{1+\omega_S^2\tau_V^2} + \frac{1}{1+\omega_S^2\tau_V^2}\right) \tag{8}$$

$$\left(\frac{1}{T_{2,e}}\right)^{ZFS} = \Delta^2\tau_V\left(\frac{5.26}{1+0.372\omega_S^2\tau_V^2} + \frac{7.18}{1+1.24\omega_S\tau_V}\right) \tag{9}$$

There S is the multiplicity of Gd^{3+} ion ($S_{Gd(III)} = 3.5$), Δ^2 is the square the zero-field splitting tensor and τ_V is the correlation time of the ZFS modulation. Considering the transient zero-filed splitting as a consequence of periodical disturbation of a complex symmetry due to collisions with solvent water molecules, Δ^2 could be seen as an amplitude and τ_V as a frequency of these disturbations.

In contrast to the ZFS mechanism, the spin-rotation relaxation pathway is field-independent and were described by Powell *at al* (Equation (10))[8]

$$\left(\frac{1}{T_{i,e}}\right)^{SR} = \frac{\delta g_L^2}{9\tau_R} \qquad \text{for } i = 1,2 \tag{10}$$

where δg_L^2 are deviations from the free electron value of the Landè g-factor along the principal axes of the g_L tensor (Equation (11))

$$\delta g_L^2 = \sum_i \delta g_{L,i}^2 \tag{11}$$

Transversal relaxation rates of bound ^{17}O nuclei $T_{2,M}$ (equation (3)) are, in contrary to the $T_{1,M}$, predominantly controlled by the scalar contribution (Equations (12) and (13))[5]:

$$\frac{1}{T_{2,c}} = \frac{1}{3}\left(\frac{A}{\hbar}\right)^2 S(S+1)\tau_{1,e} \tag{12}$$

where

$$\frac{1}{\tau_{1,e}} = \frac{1}{\tau_M} + \frac{1}{T_{1,e}} \tag{13}$$

The parameter $A/\hbar$ is the hyperfine-coupling constant of Gd-O bond usually obtained from LIS measurement[5] or from ^{17}O chemical shifts obtained for Gd(III) complex under study at variable temperature.

It was demonstrated that particularly for slowly tumbling molecules (dendrimers, proteins) at higher magnetic field, the dipolar Curie contribution to relaxation might be important. This relaxation mechanism results from an interaction of a nuclear spin with a thermal-averaged electron spin given by equations (14) and (15)[9]

$$\frac{1}{T_{1,\chi}} = \frac{6}{5}\left(\frac{\mu_0}{4\pi}\right)^2 \frac{\gamma_I^2 B \mu_{eff}^4 \beta^4}{(3kT)^2 r_{GdO}^6}\left(\frac{\tau_R}{1+\omega_I^2\tau_R^2}\right) \tag{14}$$

$$\frac{1}{T_{2,\chi}} = \frac{1}{5}\left(\frac{\mu_0}{4\pi}\right)^2 \frac{\gamma_I^2 B \mu_{eff}^4 \beta^4}{(3kT)^2 r_{GdO}^6}\left(4\tau_R + \frac{3\tau_R}{1+\omega_I^2\tau_R^2}\right) \tag{15}$$

where B is the intensity of magnetic field and k is the Boltzman constant $(1.38 \times 10^{-23}\ J\ K^{-1})$.

All mentioned relaxation mechanisms are implicitly depended on temperature as the correlation times are dynamic characteristics of a complex in solution. Whereas the temperature dependence of the rotational correlation time, τ_R, and the electronic correlation time, τ_V, are assumed to be described by an exponential functions (Equations (16) and (17)) with sufficient precision, the water residence lifetime, τ_M, is supposed to obey the Eyring equation (Equation (18)):

$$\tau_R = {}^{298}\tau_R \exp\left[\frac{E_R}{R}\left(\frac{1}{T} - \frac{1}{298.15}\right)\right] \tag{16}$$

60

$$\tau_V = {}^{298}\tau_V \exp\left[\frac{E_V}{R}\left(\frac{1}{T} - \frac{1}{298.15}\right)\right]$$ (17)

$$\tau_M = \frac{T}{{}^{298}\tau_M} \exp\left[\frac{\Delta H^{\ddagger}}{R}\left(\frac{1}{298.15} - \frac{1}{T}\right)\right]$$ (18)

where E_R, E_V and $\Delta H^{\ddagger}$ are the corresponding free energies of a reorintational motion, electronic relaxation and water exchange, respectively, and R is the universal gas constant ($R = 8.314$ J mol^{-1}K^{-1}).

^{1}H NMRD profiles

Complementary to the ^{17}O data, ^{1}H longitudinal relaxation rates are usually measured as a function of magnetic field intensity; so called NMRD profile. ^{1}H T_1 relaxation times are, as well as in ^{17}O measurements, obtained by inversion recovery experiment, although the Fast-Field Cycling (FFC) is usually involved during a measuring cycle. Likewise, the observed values are sums of several contributions given in equation (19).

$$\frac{1}{T_{1,obs}} = c_{Gd}\left(\frac{1}{T_{1,IS}} + \frac{1}{T_{1,SS}} + \frac{1}{T_{1,OS}}\right) + \frac{1}{T_{1,dia}}$$ (19)

When the ^{1}H R_1 rates are corrected for diamagnetic contribution and normalized to 1 mM concentration of Gd(III), the equation (19) could be rewritten to the form of equation (20):

$$r_1 = r_{1,IS} + r_{1,SS} + r_{1OS}$$ (20)

where $r_{1,IS}$ term could be further expand to the form of equation (21).

$$r_{1,IS} = \frac{q \times 10^{-3}}{55.56} \times \frac{1}{T_{1,M}^H + \tau_M}$$ (21)

As the protons of the coordinated water molecule do not have a direct contact with a Gd(III) ion, the inner-sphere contribution are primordially controlled by the pseudo-contact (dipolar) contribution. Mathematically, it is described by a similar equation as was written for ^{17}O data:

$$\frac{1}{T_{1,M}^H} = \frac{1}{T_{1,d}^H} = \frac{2}{15}\left(\frac{\mu_0}{4\pi}\right)^2 \frac{\gamma_I^2 \mu_{eff}^2 \beta^2}{r_{GdH}^6}\left[\frac{3\tau_{1,d}}{1+\omega_I^2\tau_{1,d}^2} + \frac{7\tau_{2,d}}{1+\omega_S^2\tau_{2,d}^2}\right] \tag{22}$$

where γ_I is the gyromagnetic ratio of proton and r_{GdH} is the average length of vector between Gd(III) ion and the protons of the coordinated water molecule. To be accurate, the rotational time of Gd-O and Gd-H vector (involved in total correlation times $\tau_{i,d}$) need not to match. In fact, the reorientational motion of Gd-H may be influenced by distinct rotation of the water molecule and Merbach at al proved that $\tau_{R,H}/\tau_{R,O}$ ratio should be around value 0.65 for simple monohydrated systems.[10] Nevertheless, an involvement of this extra-parameter is necessary only when both, the ^{17}O T_1 data and ^1H NMRD data are fitted in the same time.

It was demonstrated that in some systems (especially those with phosphorus or carboxylic amide pendants), the second-sphere term may contribute significantly to the overall proton relaxivity.[11] Similarly to the inner-sphere protons, the ones of the second-sphere interact with the Gd(III) centre only through space and then this interaction could be described by a quite similar equations (Equations (23) and (24)).

$$\frac{1}{^{SS}T_{1,M}^H} = \frac{1}{^{SS}T_{1,d}^H} = \frac{2}{15}\left(\frac{\mu_0}{4\pi}\right)^2 \frac{\gamma_I^2 \mu_{eff}^2 \beta^2}{^{SS}r_{GdH}^6}\left[\frac{3\tau_{1,d}}{1+\omega_I^2\tau_{1,d}^2} + \frac{7\tau_{2,d}}{1+\omega_S^2\tau_{2,d}^2}\right] \tag{23}$$

The total correlation times, $\tau_{i,d}$ are, in analogy with equation (6), expressed by equation (24)

$$\frac{1}{\tau_{i,d}} = \frac{1}{\tau_M^{SS}} + \frac{1}{\tau_R^{SS}} + \frac{1}{T_{i,e}} \qquad \text{for } i = 1,2 \tag{24}$$

where τ_M^{SS} and τ_R^{SS} are the corresponding correlation times of water exchange and reorientation, respectively. Their temperature functions are described by the same equations as for the inner-sphere (Equations (16) and (18)), but the exchange of water from the second-sphere is assumed to have a different free activation energy $\Delta H_{SS}^{\ddagger}$.

Finally, the outer-sphere contribution to the overall proton relaxivity are described within the Solomon-Bloembergen-Morgan theory by the Freed's equations (Equation (25) and (26)[12]:

$$r_{1,OS} = \frac{6400 N_A \pi}{81} \left(\frac{\mu_0}{4\pi}\right)^2 \frac{\hbar^2 \gamma_I^2 \gamma_S^2}{a_{GdH} D_{GdH}} S(S+1)\left[3J_{OS}\left(\omega_I, T_{1,e}\right) + 7J_{OS}\left(\omega_S, T_{2,e}\right)\right] \qquad (25)$$

where J_{OS} are the spectral density functions given by

$$J_{OS}\left(\omega, T_{j,e}\right) = \mathrm{Re}\left[\frac{1 + \frac{1}{4}\left(i\omega\tau + \frac{\tau}{T_{j,e}}\right)^{1/2}}{1 + \left(i\omega\tau + \frac{\tau}{T_{j,e}}\right)^{1/2} + \frac{4}{9}\left(i\omega\tau + \frac{\tau}{T_{j,e}}\right) + \frac{1}{9}\left(i\omega\tau + \frac{\tau}{T_{j,e}}\right)^{3/2}}\right] \quad \text{for } j = 1,2 \quad (26)$$

The parameter τ is defined as the ratio a_{GdH}^2/D, where a_{GdH} is the closest distance the water molecules can get by mere diffusion motion and D is the corresponding diffusion coefficient. For calculation of its value, I have used the semiempirical Hindman's equation[13] but the exponential temperature dependence similar to that for the reorintational correlation time (Equation (16) is also frequently.

<div align="center">

Lipari-Szabo modification

</div>

The substantial difference between the Bloembergen-Solomon-Morgan equations and the Lipari-Szabo ones lies in a separation of a molecular tumbling into two distinct motions: the global one and the internal one represented by two rotational correlation times τ_{Rg} and τ_{Rl}.[14] Consequently, all contributions to the relaxivity that are correlated with the molecular motion need to be modified. Notably, this modification affects mainly a treatment of an NMRD profile and ^{17}O T_1 data as the T_2 ^{17}O data are controlled by a contact interaction where the rotational correlation time is not involved. Practically, the total dipolar correlation time needs to be split according to equations (27) and (28)

$$\frac{1}{\tau_{i,d}^g} = \frac{1}{\tau_M} + \frac{1}{\tau_R^g} + \frac{1}{T_{i,e}} \qquad (27)$$

$$\frac{1}{\tau_{i,d}^l} = \frac{1}{\tau_M} + \frac{1}{\tau_R^{tot}} + \frac{1}{T_{i,e}} \qquad \text{for } i = 1, 2 \qquad (28)$$

where τ_R^{tot} is defined as the superposition of both the global and the local motions given by the equation (29):

$$\frac{1}{\tau_R^{tot}} = \frac{1}{\tau_R^g} + \frac{1}{\tau_R^l} \tag{30}$$

Then, the inner-sphere contribution to the proton relaxivity (controlled by the dipolar term) is given by the equation (30):

$$r_{1,IS} = \frac{2}{15}\left(\frac{\mu_0}{4\pi}\right)^2 \frac{\gamma_I^2 \mu_{eff}^2 \beta^2}{r_{GdO}^6}\left[\begin{array}{l} 3\left\{S^2\left(\dfrac{\tau_{1,d}^g}{1+\omega_I^2 \tau_{1,d}^{g\,2}}\right) + \left(1-S^2\right)\left(\dfrac{\tau_{1,d}^l}{1+\omega_I^2 \tau_{1,d}^{l\,2}}\right)\right\} + \\[2em] 7\left\{S^2\left(\dfrac{\tau_{2,d}^g}{1+\omega_S^2 \tau_{2,d}^{g\,2}}\right) + \left(1-S^2\right)\left(\dfrac{\tau_{2,d}^l}{1+\omega_S^2 \tau_{2,d}^{l\,2}}\right)\right\} \end{array}\right] \tag{29}$$

where S^2 is the Lipari-Szabo rigidity term that can vary between 1 for totally rigid molecules to 0 for totally flexible ones. It should be noted, that in the other equations where the τ_R is included (like in the second-sphere equations (23), the equations for the spin-rotation (10) and/or in the equation for the Curie contribution (14) and (15)), the τ_R^{tot} is just substituted for simple τ_R.

References:

[1] K. Mickskei, L. Helm, E. Brücher and A. E. Merbach, *Inorg. Chem.* **1993**, *32*, 3844.

[2] T. J. Swift and R. E. Connick, *J. Chem. Phys.* **1962**, *37*, 307.

[3] R. L. Vold, J. S. Waugh, M. P. Klein and D. E. Phelps, *J. Chem, Phys.* **1968**, *43*, 3831.

[4] S. Meiboom and D. Gill, *Sci. Instrum.* **1958**, *29*, 688.

[5] J. A. Peters, J. Huskens and D. J. Raber, *Prog. NMR Spectrosc.* **1996**, *32*, 283.

[6] I. Solomon, Phys. Rev. **1995**, *99*, 559.

[7] N. Bloembergen and L. O. Morgan, *J. Phys. Chem.* **1961**, *34*, 842.

[8] G. González, D. H. Powell, V. Tissières, A. E. Merbach, *J. Phys. Chem.* **1994**, *98*, 53.

[9] a) M. Gueron, J. Magn. Reson. **1975**, *19*, 58; b) A. J. Vega and D. Fiat, *Mol. Phys.* **1976**, *31*, 347.

[10] a) F. A. Dunand, A. Borel and A. E. Merbach, *J. Am. Chem. Soc.* **2002**, *124*, 710; b) F. Yerly, K. Hardcastle, L. Helm, S. Aime, M. Botta and A. E. Merbach, *Chem. Eur. J.* **2002**, *8*, 1031.

[11] a) A. Barge, M. Botta, D. Parker and H. Puschmann, *Chem. Commun.* **2003**, 1386; b) S. Aime, M. Botta, E. Garino, S. G. Crich, G. Giovenzana, R. Pagliarin, G. Palmisano and M. Sisti, *Chem. Eur. J.* **2000**, *6*, 2609; c) S. Aime, A. S. Batsanov, M. Botta, R. S. Dickins, S. Falkner, C. E. Foster, A. Harrison, J. A. K. Howard, J. M. Moloney, T. J. Norman, D. Parker and J. A. G. Williams, *J. Chem. Soc. Dalton Trans.* **1997**, 3623.

[12] J. H. Freed, *J. Chem. Phys.* **1978**, *68*, 4034.

[13] J. C. Hindman, *J. Chem. Phys.* **1974**, 60, 4488.

[14] a) G. Lipari and S. Szabo, *J. Am. Chem. Soc.* **1982**, *104*, 4546; b) G. Lipari and S. Szabo, *J. Am. Chem. Soc.* **1982**, *104*, 4559.